

# Heterogeneous CO<sub>2</sub> and CH<sub>4</sub> content of glacial meltwater from the Greenland Ice Sheet and implications for subglacial carbon processes

Andrea J. Pain<sup>1,2</sup>, Jonathan B. Martin<sup>1</sup>, Ellen E. Martin<sup>1</sup>, Åsa K. Rennermalm<sup>3</sup>, Shaily Rahman<sup>1,4</sup>

<sup>1</sup> University of Florida, Department of Geological Sciences, Gainesville, FL 32611

<sup>2</sup> Now at: University of Maryland Center for Environmental Science, Horn Point Lab, Cambridge, MD 21613

<sup>3</sup> Rutgers, The State University of New Jersey, Department of Geography, Piscataway NJ 08854

<sup>4</sup> Now at: University of Southern Mississippi, Department of Marine Science, Stennis Space Center, MS 39529

Correspondence to: Andrea J. Pain (apain@umces.edu)

10 **Abstract.** Accelerated melting of the Greenland Ice Sheet has increased freshwater delivery to the Arctic Ocean and amplified the need to understand the impact of Greenland Ice Sheet meltwater on Arctic greenhouse gas budgets. We **evaluate subglacial discharge from the Greenland Ice Sheet for** carbon dioxide (CO<sub>2</sub>) and methane (CH<sub>4</sub>) concentrations and δ<sup>13</sup>C values **in order** to evaluate subglacial CH<sub>4</sub> and CO<sub>2</sub> sources and sinks **using geochemical models. We compare discharge from** southwest (a sub-catchment of the Isunnguata Glacier, sub-Isunnguata, and the Russell Glacier) and southern Greenland (Kiattut Sermiat).

15 Meltwater CH<sub>4</sub> concentrations vary by orders of magnitude between sites and are saturated with respect to atmospheric concentrations at Kiattut Sermiat. In contrast, **meltwaters from** southwest sites **are** supersaturated, even though oxidation reduces CH<sub>4</sub> concentrations by up to 50% during periods of low discharge. CO<sub>2</sub> concentrations range from supersaturated at sub-Isunnguata to undersaturated at Kiattut Sermiat. CO<sub>2</sub> is consumed by mineral weathering throughout the melt season at all sites, however differences in the magnitude of subglacial CO<sub>2</sub> sources result in meltwaters that are either sources or sinks of

20 atmospheric CO<sub>2</sub>. At the sub-Isunnguata site, the predominant source of CO<sub>2</sub> is organic matter (OM) remineralization. **However,** multiple or heterogeneous subglacial CO<sub>2</sub> sources maintain atmospheric CO<sub>2</sub> concentrations at Russell but not at Kiattut Sermiat where CO<sub>2</sub> is undersaturated. These results highlight a previously unrecognized degree of heterogeneity in greenhouse gas dynamics under the Greenland Ice Sheet. Future work should constrain the extent and controls of heterogeneity to improve our understanding of the impact of Greenland Ice Sheet melt on Arctic greenhouse gas budgets, as well as the role

25 of continental ice sheets in greenhouse gas variations over glacial-interglacial timescales.

## 1 Introduction

Glaciers play an important role in global chemical cycles due to the production of fine-grained sediments that participate in carbonate and silicate mineral weathering reactions (Table 1), which are the principal sink of atmospheric CO<sub>2</sub> over geologic timescales (Berner et al., 1983; Walker et al., 1981). Variations in the weathering intensity of comminuted

30 sediments may contribute to glacial-interglacial atmospheric CO<sub>2</sub> variations as sediments are alternately covered by ice and

**Style Definition:** Default Paragraph Font

**Deleted:** Heterogenous

**Deleted:** measured

**Deleted:** and use geochemical models

**Deleted:** in water discharging from three subglacial outlets of the Greenland Ice Sheet in

**Deleted:** ;

**Deleted:** meltwater in

**Deleted:** is

**Deleted:** At Russell and Kiattut Sermiat sites

**Deleted:** that

exposed following ice retreat. However, the importance of CO<sub>2</sub> consumption by mineral weathering is poorly understood, including effects from the advance and retreat of continental ice sheets (Ludwig et al., 1999). Recent evaluations of carbon budgets in proglacial environments indicate that mineral weathering results in net sequestration of atmospheric CO<sub>2</sub>, suggesting that proglacial systems are underrecognized as Arctic CO<sub>2</sub> sinks (St Pierre et al., 2019), however alternate processes could lead to the production of greenhouse gases in glacial systems. For instance, CH<sub>4</sub> production in anaerobic subglacial environments driven by the remineralization of organic matter (OM) contained in soils and forests covered during glacial margin fluctuations has been suggested as a potential carbon feedback to drive warming (Sharp et al., 1999; Wadham et al., 2008). Because the global warming potential of CH<sub>4</sub> is 25 times greater than CO<sub>2</sub>, even limited subglacial methanogenesis has the potential to strongly impact the greenhouse gas composition of glacial meltwater. Combined inorganic and organic subglacial processes may therefore produce glacial meltwater that is a source or sink of greenhouse gas. While the net impact of these processes on modern carbon fluxes is poorly constrained, determining these impacts will improve modern carbon budgets as well as depictions of how fluxes may have evolved during the advance and retreat of continental ice sheets.

In subglacial environments where remineralization is limited by low OM availability, the major element solute load of glacial meltwater is typically dominated by products of mineral weathering reactions (Tranter, 2005). The extent of mineral weathering in subglacial environments depends in part on the availability of acids to drive reactions, namely sulfuric and carbonic acids (Table 1). Sulfuric acid is derived from the oxidation of reduced sulfur species, which largely occur as iron-sulfide minerals including pyrite (Tranter, 2005). Sulfide oxidation may occur abiotically; however, the kinetics of microbially mediated sulfide oxidation is several orders of magnitude faster and may lead to local depletion of oxygen given a sufficient supply of sulfide minerals (Sharp et al., 1999). In contrast, carbonic acid may be derived from multiple external or *in situ* sources of CO<sub>2</sub> to the system. The dominant external source is supraglacial meltwater that flows to the subglacial system through moulins following equilibration with atmospheric CO<sub>2</sub> (Fig. 1). Unlike proglacial environments where free exchange between water and the atmosphere may resupply CO<sub>2</sub> consumed by weathering, subglacial environments may be partially or fully isolated from the atmosphere, limiting further atmospheric CO<sub>2</sub> invasion and thus the extent of mineral weathering with carbonic acid. However, additional atmospheric CO<sub>2</sub> may be delivered in open portions of the subglacial environment through exchange in fractures or moulins along subglacial flow paths or in partially air-filled conduits, allowing a much greater magnitude of carbonic acid mineral weathering (Graly et al., 2017). CO<sub>2</sub> may also be derived from *in situ* sources, such as gaseous CO<sub>2</sub> contained in ice bubbles of basal ice, or fluid inclusions in rocks that release volatiles (including CO<sub>2</sub>) following mechanical grinding (Macdonald et al., 2018). When OM is available, its remineralization also generates CO<sub>2</sub> (and potentially CH<sub>4</sub>) along with nutrients, but low OM availability in many subglacial systems limits remineralization as a CO<sub>2</sub> source (Fig. 1).

The role of subglacial carbon processes may play an increasingly important role in modern Arctic carbon budgets as disproportionate warming increases glacial meltwater and sediment fluxes to the ocean, particularly from the Greenland Ice Sheet (Wadham et al., 2019). The is the last remaining ice sheet in the Northern Hemisphere following collapse of other ice

**Deleted:** The role of subglacial carbon processes may play an increasingly important role in modern Arctic carbon budgets as disproportionate warming increases glacial meltwater and sediment fluxes to the ocean, particularly from the Greenland Ice Sheet. The is the last remaining ice sheet in the Northern hemisphere

80 sheets since the Last Glacial Maximum (~20 ka). It has been losing mass at increasing rates that averaged  $286 \pm 20$  Gt/yr  
85 between 2010-2018, representing a six-fold increase since the 1980s (Mouginot et al., 2019). While mineral weathering  
significantly modifies the chemical composition of Greenland Ice Sheet subglacial discharge (e.g. Hindshaw et al., 2014;  
Deuerling et al., 2018; Urra et al., 2019) and should consume CO<sub>2</sub> similar to other glacial and proglacial environments, the  
recent identification of microbially driven reactions (including methanogenesis) in subglacial environments of the Greenland  
Ice Sheet indicates that organic processes may also play a role (Dieser et al., 2014; Lamarche-Gagnon et al., 2019). The relative  
importance of subglacial greenhouse gas sinks (CO<sub>2</sub> consumption through mineral weathering) and sources (such as OM  
remineralization) determine the greenhouse gas composition of subglacial discharge, which may then serve as a source or a  
sink of atmospheric greenhouse gases. Constraining the relative impacts and variability of these processes underneath the  
Greenland Ice Sheet will provide important information regarding the current and future impact of Greenland Ice Sheet loss  
on Arctic carbon budgets, as well the role of continental ice sheets on carbon cycle feedbacks.

**Deleted:** (Dieser et al., 2014; Lamarche-Gagnon et al., 2019; Musilova et al., 2017).

90 To evaluate the net impact of carbon processes on the greenhouse gas composition of subglacial discharge of the  
Greenland Ice Sheet, we compare water chemistry, dissolved CO<sub>2</sub> and CH<sub>4</sub> concentrations, and gas stable isotopic compositions  
between three subglacial discharge sites draining land-terminating glaciers of the Greenland Ice Sheet over the melt seasons  
of 2017 and 2018 (Fig. 2). We employ mass balance models utilizing the concentrations of major cations and anions to  
determine the magnitude of the impact on CO<sub>2</sub> concentrations from mineral weathering reactions (Table 1). These results are  
95 combined with measured gas concentrations and  $\delta^{13}\text{C}$  to determine the relative importance of mineral weathering compared  
to OM remineralization on the CH<sub>4</sub> and CO<sub>2</sub> content of subglacial discharge. We also assess the temporal and spatial variability  
of these processes under the Greenland Ice Sheet to improve our understanding of carbon cycling in Greenland subglacial  
environments and the implications of Greenland Ice Sheet mass loss on Arctic carbon budgets.

## 2 Methods

### 100 2.1 Study locations

Our three subglacial discharge locations are located in southwest (Fig. 2a, b) and southern (Fig. 2a, c) Greenland  
(pictures given in Supplementary Material). Our sub-Isunnguata watershed (IS; 67°09'27.1" N, 50°03'25.0" W) and Russell  
Glacier watershed (RU; 67°05'22.1" N, 50°14'18.7" W) drain to the Akuliarusiarsuup Kuua, which is a tributary to the  
Qinnguata Kuussua. The short stretch of river downstream of the confluence of the Akuliarusiarsuup Kuua and the main stem  
105 of the Qinnguata Kuussua near the town of Kangerlussuaq is also known as the Watson River (Fig. 2b). The majority of  
drainage from the Isunnguata Glacier drains to the northern Isortoq River (Fig. 2), however a sub-catchment of the Isunnguata  
drains to a stream that directly feeds the Akuliarusiarsuup Kua, which we refer to as the Northern Tributary, while the  
Akuliarusiarsuup Kuua refers to river that flows between the outlet of the Russell Glacier and the confluence with the  
Qinnguata Kuussua (Fig. 2b). Watson River discharge is monitored by PROMICE (Programme for Monitoring of the  
110 Greenland Ice Sheet; van As et al., 2018) and total discharge was 4.3 and 3.6 km<sup>3</sup> of water in 2017 and 2018, respectively (van

**Deleted:** thecQinnguata

As et al., 2018). The total catchment size for the Isunnguata is 15,900 km<sup>2</sup>, though the size of the sub-catchment draining to the Northern Tributary is much smaller with a drainage area of approximately 40 km<sup>2</sup> (Lindbäck et al., 2015; Rennermalm et al., 2013), therefore we hereby refer to this site as the sub-Isunnguata watershed. The total drainage area for the Russell glacier is not precisely known, however the catchment draining both the Russell and Leverett glaciers has been estimated at approximately 900 km<sup>2</sup> (Lindback et al., 2015) while the Leverett drainage area alone is estimated at approximately 600 km<sup>2</sup> (Hawkings et al., 2016). We therefore estimate the Russell drainage area at approximately 300 km<sup>2</sup>, though may be considerably smaller (van de Wal and Russell, 1994). Discharge from the third site in southern Greenland, Kiattut Sermiat (KS; 61°12'13.5" N, 45°19'49.1"W) drains to the Kuusuaq River near the town of Narsarsuaq. While Kuusuaq discharge is not monitored, a previous study using dye tracing techniques estimated approximately 0.22 km<sup>3</sup> of discharge in 2013, and its catchment size was estimated at 36 km<sup>2</sup> (Hawkings et al., 2016).

Underlying lithologies differ between sites. Southwest Qinnuata Kuussua sites are located near the boundary between the Archean Craton to the south and the southern Nagssugtoqidian Orogen to the north (Henriksen et al., 2009). The Archean Block is composed of granites and granulite facies orthogneisses that were intruded by mafic dykes during Paleoproterozoic rifting. These rocks were deformed and modified during subsequent continent-to-continent collision in the Paleoproterozoic to create the amphibolite facies gneisses of the southern Nagssugtoqidian Orogen (van Gool et al., 2002). Kiattut Sermiat lies within the Paleoproterozoic Ketilidian fold belt (Henriksen et al., 2009). Lithologies in this region include the Julianehåb Granite and associated basic intrusions and the sedimentary and volcanic rocks of the Mesoproterozoic Gardar Province that include a suite of alkaline igneous rocks and basaltic dykes with interbedded sandstones (Kalsbeek and Taylor, 1985; Upton et al., 2003).

Previous studies have characterized chemical weathering reactions in subglacial discharge to the Akuliarusiarsuup Kua and Qinnuata Kuussua (Deuerling et al., 2018; Hasholt et al., 2018; Yde et al., 2014), in the Kuusuaq that drains Kiattut Sermiat (Hawkings et al., 2016), and in comparison between these two sites (Urra et al., 2019). There has been extensive work regarding ice sheet dynamics and hydrology in the southeast glaciers draining to the Akuliarusiarsuup Kua and Qinnuata Kuussua (Van As et al., 2017, 2018; Lindbäck et al., 2015) as well as southern Kuusuaq catchments (Warren and Glasser, 1992; Winsor et al., 2014). Subglacial permafrost has been identified near the sub-Isunnguata site (Ruskeeniemi et al., 2018) and mostly likely formed during Holocene fluctuations in the ice sheet margin. While a similar Holocene ice retreat and re-advance may have occurred in southern Greenland (Larsen et al., 2016), it is unknown whether this retreat led to the organic deposits below the ice sheet.

## 2.2 Sample collection

We collected water samples from subglacial discharge sites in spring and fall of 2017, and the summer of 2018 to observe seasonal variations in water chemistry. To minimize atmospheric influence, samples were collected as close as possible to the glacier front where subglacial waters emerge, which was less than 10 m for the sub-Isunnguata site and approximately 100 m for the Russell glacier site. Subglacial discharge from Kiattut Sermiat site flowed through a glacial meltwater lake prior

**Deleted:** , therefore we estimate the Russell drainage area at approximately 300 km<sup>2</sup>.

**Deleted:**

150 to arriving at the sampling location, which was approximately 1.1 km from the glacial outlet (Fig. 2) and therefore may  
experience a more interaction with atmospheric gases during transport from the subglacial discharge site to our sampling  
location. We collected water samples by pumping water through a 0.5-cm flexible PVC tube that was placed in flowing water  
as far as possible from shore (approximately 1-2 m). A YSI Pro-Plus sensor that was calibrated daily was installed in an  
overflow cup filled from the bottom to measure specific conductivity (Sp.C), temperature, pH, dissolved oxygen, and  
155 oxidation-reduction potential (ORP). These parameters were monitored until stable, between about 10 and 30 minutes, after  
which samples were collected and preserved in the field according to the solute to be measured after being filtered through a  
0.45  $\mu\text{m}$  trace-metal grade Geotech high-capacity disposable canister filter. Samples for cations and anions were collected in  
HDPE bottles; cation samples were preserved with Optima-grade ultrapure nitric acid ( $\text{pH} < 2$ ) while no preservative was added  
to anion samples. Dissolved inorganic carbon (DIC) samples were filtered through 0.2  $\mu\text{m}$  filters directly to the bottom of 20  
160 ml Qorpac glass vials and allowed to overflow until sealed tightly with no headspace.

Gas samples were collected in duplicate via headspace extractions according to methods outlined in Repo et al. (2007)  
and Pain et al. (2019). Unfiltered water was pumped into the bottom of 500 mL bottles until they overflowed. Bottles were  
immediately capped with rubber stoppers fitted with two 3-way inlet valves. 60 mL of water was extracted from one inlet and  
replaced with 60 mL of atmospheric air (for spring and fall 2017 sampling trips) or ultrapure  $\text{N}_2$  gas in a gas bag (summer  
165 2018 sampling trip). Bottles were shaken for 2 minutes to equilibrate headspace gas with water, and headspace gas was  
extracted and immediately injected into 60 ml glass serum bottles that had been evacuated immediately prior to sample  
introduction. Samples were stored at room temperature until analysis, which occurred within one week of collection. Measured  
headspace concentrations were converted to dissolved concentrations using methods outlined in Pain et al. (2019). When  
atmospheric air was used for headspace extractions, atmosphere samples were collected in tandem and analyzed to correct the  
170 calculated dissolved  $\text{CO}_2$  and  $\text{CH}_4$  concentrations and isotopic compositions for atmospheric  $\text{CO}_2$  and  $\text{CH}_4$ . This correction  
altered  $\text{CH}_4$  concentrations by up to 22% for one sample from the Russell glacier, though less than 5% for all other samples,  
and resulted in a correction of  $\delta^{13}\text{C}\text{-CH}_4$  of up to 1.3‰. For  $\text{CO}_2$ , the correction altered concentrations by up to 15% for one  
sample collected at Kiattut Sermiat, though less than 10% for all other samples, and resulted in a correction of  $\delta^{13}\text{C}\text{-CO}_2$  of  
up to 0.4‰.

175 In samples collected in fall 2017 and summer 2018, alkalinity was measured in the field laboratory within 3 days of  
collection by titration with 0.01 N HCl using the Gran method. Because alkalinity measurements were not available for the  
spring 2017 sampling trip, we estimate alkalinity with PHREEQc modeling and the phreeqc.dat database (Parkhurst, 1997)  
using major cations and anions, pH, temperature, and DIC concentrations as model inputs.

### 2.3 Laboratory analysis

180 Gas samples were analyzed for  $\text{CO}_2$  and  $\text{CH}_4$  concentrations, and  $\delta^{13}\text{C}\text{-CO}_2$  and  $\delta^{13}\text{C}\text{-CH}_4$  on a Picarro G2201-i cavity  
ring-down spectrometer in the field within a few days of collection. Carbon isotopic compositions are reported in reference to  
Vienna Pee Dee Belemnite (VPDB). Check standards of known  $\text{CO}_2$  and  $\text{CH}_4$  concentrations and isotopic compositions were

measured during each sample run and were accurate within 10%. Anion and cation concentrations were measured on an automated Dionex ICS-2100 and ICS-1600 Ion Chromatograph, respectively. Error on replicate analyses was less than 5%.

185 DIC concentrations were measured on a UIC (Coulometrics) 5011 CO<sub>2</sub> coulometer coupled with an AutoMate Preparation Device. Samples were acidified and the evolved CO<sub>2</sub> was carried through a silver nitrate scrubber to the coulometer where total C was measured. Accuracy was calculated to be ±0.1 mg/L based on measurement of check standards.

## 2.4 Methane modeling

To assess CH<sub>4</sub> sources and sinks, we calculate  $\epsilon_c$ , or the carbon isotopic fractionation factor between CO<sub>2</sub> and CH<sub>4</sub> as defined in Whiticar (1999):

$$\epsilon_c = \delta^{13}C_{CO_2} - \delta^{13}C_{CH_4} \quad (5)$$

Values of  $\epsilon_c$  reflect methanogenesis pathways (acetoclastic or CO<sub>2</sub> reduction) as well as the extent of oxidation. Values of  $\epsilon_c$  between approximately 40 and 55‰ are produced for CH<sub>4</sub> generated via acetoclastic methanogenesis, while CO<sub>2</sub> reduction produces values between approximately 55 and 90‰. Lower values ( $\epsilon_c$  between 5 and 30) result when CH<sub>4</sub> oxidation predominates. Modern atmospheric input without additional alteration of CO<sub>2</sub> or CH<sub>4</sub> isotopic systematics results in a  $\epsilon_c$  value of approximately 40 (Whiticar, 1999).

We calculated CH<sub>4</sub> oxidation using the isotopic method outlined in Mahieu et al. (2008) and Preuss et al. (2013). The fraction of oxidized methane ( $f_{ox}$ ) in an open system is given by:

$$f_{ox} = \frac{\delta_E - \delta_P}{1000 \cdot (\alpha_{ox} - \alpha_{trans})} \quad (6)$$

where  $\delta_E$  is the measured  $\delta^{13}C$ -CH<sub>4</sub> value for each water sample,  $\delta_P$  is  $\delta^{13}C$ -CH<sub>4</sub> of produced methane,  $\alpha_{ox}$  is the oxidation fractionation factor, and  $\alpha_{trans}$  is a fractionation factor resulting from diffusive transportation of CH<sub>4</sub>. While the exact value of  $\delta_P$  is unknown, diagenetic alteration of  $\delta^{13}C$ -CH<sub>4</sub> values through oxidation or transport only enrich  $\delta^{13}C$ -CH<sub>4</sub> signatures, therefore the value of  $\delta_P$  is taken as the most depleted  $\delta^{13}C$ -CH<sub>4</sub> signature assuming it is the least impacted by diagenetic alteration. Literature-reported values for  $\alpha_{ox}$  range between 1.003 and 1.049. We calculate the fraction of oxidized methane with the largest fraction factor ( $\alpha_{ox} = 1.049$ ; Mahieu et al., 2008), which yields the minimum amount of CH<sub>4</sub> oxidation required to explain the observed variations in  $\delta^{13}C$ , and thus is a conservative estimate for CH<sub>4</sub> oxidation, and actual oxidation ratios may be higher. Literature-reported values for  $\alpha_{trans}$  vary from 1 for advection-dominated systems to 1.0178 for diffusion-dominated porous media (Visscher et al., 2004; Mahieu et al., 2008; Preuss et al., 2013). We assume that transport is advection dominated and thus assume  $\alpha_{trans} = 1$ , however diffusive transport of CH<sub>4</sub> may result in fractionation of CH<sub>4</sub> in the subglacial environment and lead to relatively lower estimates of  $f_{ox}$ . Because hydrologic connectivity between subglacial methanogenic meltwater pockets and drainage features is not well described, the relative importance of advective compared to diffusive CH<sub>4</sub>

transport within the subglacial drainage system is not well understood; however, it is presumed to be an advection-dominated system in which expanding drainage networks access and drain methanogenic meltwater pockets throughout the melt season.

## 2.5 Mineral weathering and carbonate modeling

We used major cation and anion concentrations and alkalinity to partition solutes into the four mineral weathering reactions in Table 1 after correcting solute concentrations for marine aerosol deposition using measured chloride concentrations and standard seawater element ratios. The mass balance model followed the methods of Deuerling et al. (2019). After apportioning solutes to mineral weathering reactions, we used the stoichiometries of reactions to calculate the impact of each reaction on dissolved CO<sub>2</sub> concentrations (Table 1). The mineral weathering model apportions solutes to reactions in Table 1 based on the ratios of Ca/Na and Mg/Na in silicate minerals in stream bedload samples, which were taken to be 0.54 and 0.38, respectively, for sub-Isunnguata and Russell Glacier samples (Deuerling et al., 2019; Hindshaw et al., 2014; Wimpenny et al., 2010, 2011) and 0.39 and 0.27, respectively, for Kiattut Sermiat samples (Da Prat and Martin, 2019). Because mineral weathering reactions may both add and remove CO<sub>2</sub>, we discuss both the net impact of mineral weathering on CO<sub>2</sub> concentrations (Net CO<sub>2-MW</sub>), which may have a positive or negative value:

$$[\text{Net CO}_{2\text{-MW}}] = [\text{CO}_{2\text{-CarbCA}}] + [\text{CO}_{2\text{-CarbSA}}] + [\text{CO}_{2\text{-SilCA}}] \quad (7)$$

as well as the total impact of mineral weathering on CO<sub>2</sub> concentrations (Total CO<sub>2-MW</sub>),

$$[\text{Total CO}_{2\text{-MW}}] = |[\text{CO}_{2\text{-CarbCA}}]| + |[\text{CO}_{2\text{-CarbSA}}]| + |[\text{CO}_{2\text{-SilCA}}]| \quad (8)$$

where changes in the concentrations of CO<sub>2</sub> are defined by their absolute values. To discuss the relative importance of individual reactions, we define proportional contributions of each reaction as follows:

$$\% \text{CO}_{2\text{-CarbCA}} = \frac{|[\text{CO}_{2\text{-CarbCA}}]|}{[\text{Total CO}_{2\text{-MW}}]} * 100 \quad (9a)$$

$$\% \text{CO}_{2\text{-CarbSA}} = \frac{|[\text{CO}_{2\text{-CarbSA}}]|}{[\text{Total CO}_{2\text{-MW}}]} * 100 \quad (9b)$$

$$\% \text{CO}_{2\text{-SilCA}} = \frac{|[\text{CO}_{2\text{-SilCA}}]|}{[\text{Total CO}_{2\text{-MW}}]} * 100 \quad (9c)$$

We combine measured CO<sub>2</sub> concentrations with Net CO<sub>2-MW</sub> in order to determine the magnitude of CO<sub>2</sub> production or consumption in the subglacial environment due to processes besides mineral weathering. This analysis assumes that the concentration of CO<sub>2</sub> measured at the subglacial outlet is equivalent to the net change in CO<sub>2</sub> due to mineral weathering plus the sum of all other subglacial CO<sub>2</sub> sources and sinks. We refer to the sum of all other subglacial CO<sub>2</sub> sources and sinks as CO<sub>2-total</sub>, which represents the amount of CO<sub>2</sub> that must have been supplied to the subglacial environment to balance the mineral weathering CO<sub>2</sub> sink:

$$\text{CO}_{2\text{-measured}} = \text{Net CO}_{2\text{-MW}} + \text{CO}_{2\text{-total}} \quad (10)$$

The sources of CO<sub>2</sub> to CO<sub>2-total</sub> may be evaluated through the use of Keeling plots, which are constructed as the inverse  
240 of CO<sub>2</sub> concentrations ([CO<sub>2</sub>]<sup>-1</sup>) versus stable isotopic composition (δ<sup>13</sup>C-CO<sub>2</sub>). If variations in the concentration and isotopic  
composition of CO<sub>2</sub> arise from the mixing of two CO<sub>2</sub> reservoirs with constant isotopic compositions and concentrations  
(Keeling, 1958), a linear relationship is expected between [CO<sub>2</sub>]<sup>-1</sup> and δ<sup>13</sup>C-CO<sub>2</sub>. The y-intercept of a regression between these  
variables represents the isotopic composition of the high-CO<sub>2</sub> end member. Because measured CO<sub>2</sub> concentrations include  
both subglacial CO<sub>2</sub> sources and sinks, which may include considerable consumption through mineral weathering reactions,  
245 the magnitude of the total subglacial CO<sub>2</sub> source is taken as CO<sub>2-total</sub>. We therefore construct Keeling plots between [CO<sub>2-total</sub>]<sup>-1</sup>  
and measured δ<sup>13</sup>C-CO<sub>2</sub> values because while mineral weathering impacts the concentration of CO<sub>2</sub>, its isotopic composition  
is not appreciably altered (Myrntinen et al., 2012) compared to the range of isotopic compositions of potential CO<sub>2</sub> end  
members, namely OM remineralization, atmospheric CO<sub>2</sub>, and lithogenic CO<sub>2</sub> sources due to mechanical grinding (Fig. 1).

## 2.6 Discharge relationships

250 We evaluate the relationship between subglacial CH<sub>4</sub> and CO<sub>2</sub> dynamics and glacial meltwater river discharge  
records collected downstream of the sub-Isunnguata and upstream of the Russell sampling sites. Proglacial river discharge  
was collected in the Akuliarusiarsuup Kuua (AK) River at the AK4 site, 2 km downstream of the sub-Isunnguata sampling  
site (Fig. 2b). The river discharge dataset is an updated and extended version of [Rennermalm et al. \(2012\)](#)  
using reference and regression models to correct Solinst level logger drift in water stage (Solinst, 2017), and a total of 57  
255 discharge measurements to convert continuous water stage to discharge. The standard uncertainty (i.e. the 68<sup>th</sup> percent  
confidence interval or one standard deviation) was determined to be 17% using methods and recommendations provided by  
(Hersch, 1999; ISO Guide 98-3, 2008; WMO, 2010).

Because diurnal fluctuations in river discharge can be large, and differing water travel times from subglacial outlet  
sites to the discharge monitoring site induces a lag between maximum daily discharge at subglacial discharge sites and the  
260 AK4 site outlet, we compare subglacial CH<sub>4</sub> and CO<sub>2</sub> concentrations to average daily discharge, calculated as the average of  
hourly discharge estimates over the days on which subglacial discharge water samples were collected. We use the AK4 site  
discharge records for evaluating concentration-discharge relationships for both sub-Isunnguata and Russell sites. Although this  
site is upstream of the Russell Glacier, its close proximity to the Russell Glacier suggests it is more likely to reflect local  
melting patterns similar to those that would be controlling discharge dynamics at the Russell than discharge records collected  
265 at the Watson River outlet. While Watson River discharge records are also available through PROMICE (van As et al., 2018),  
which includes some contributions from the Russell glacier, the Watson River includes discharge from the Akuliarusiarsuup  
Kuua (draining sub-Isunnguata, Russell, and Leverett catchments) as well as the much larger Qinguata Kuussua catchment  
and therefore Watson River discharge records are not likely to be representative of the temporal changes in the magnitude and  
variability of discharge from the much smaller Russell glacier catchment.

Deleted: Rennermalm et al. (2012)



### 3 Results

#### 3.1 Temporal variability in water chemistry and gas concentrations

Chemical parameters differ spatially between subglacial discharge sites as well as temporally through the 2017-2018 melt seasons. Comparing the means and standard deviations of water samples collected throughout 2017 and 2018, specific conductivity (Sp.C; Fig. 3a) is typically highest at Kiattut Sermiat ( $26\pm 8$   $\mu\text{S}/\text{cm}$ ), followed by Russell ( $22\pm 5$   $\mu\text{S}/\text{cm}$ ) and sub-Isunnguata sites ( $13\pm 9$   $\mu\text{S}/\text{cm}$ ; Fig. 3a). All sites show variability over time, with lowest values occurring in the summer for sub-Isunnguata and Russell, while Sp.C drops continuously with days of the year for Kiattut Sermiat. Sites differ in pH, and average values at Kiattut Sermiat ( $8.2\pm 0.4$ ) are higher than both Russell ( $7.2\pm 0.2$ ) and sub-Isunnguata ( $6.6\pm 0.6$ ; Fig. 3b), and while values vary over time, no consistent trend is identified between sites. The saturation of dissolved oxygen (D.O.) with respect to atmospheric concentrations is similar between sites, though sub-Isunnguata ( $98\pm 8\%$ ) values fall below Russell ( $115\pm 16\%$ ) and Kiattut Sermiat ( $117\pm 11\%$ ) during all sampling times and exhibit undersaturation in the mid-summer samples, while Russell and Kiattut Sermiat are consistently supersaturated (Fig. 3c). Alkalinity is similar at Russell ( $93\pm 31$   $\mu\text{eq}/\text{L}$ ) and Kiattut Sermiat ( $93\pm 26$   $\mu\text{eq}/\text{L}$ ) which are higher than at sub-Isunnguata ( $39\pm 25$   $\mu\text{eq}/\text{L}$ ), but all reach minimum values in summer (Fig. 3d).  $\text{CH}_4$  concentrations differ by orders of magnitude between sites (Fig. 3e) and are consistently supersaturated with respect to atmospheric concentrations at sub-Isunnguata ( $648\pm 411$  ppm or  $1575\pm 997$  nM) and Russell ( $58\pm 33$  ppm or  $110\pm 78$  nM) sites, while close to atmospheric equilibrium at Kiattut Sermiat ( $4\pm 2$  ppm or  $9\pm 5$  nM). Mean  $\delta^{13}\text{C}-\text{CH}_4$  values (Fig. 3f) are similar between sub-Isunnguata ( $-54.7\pm 7.5\%$ ), Russell ( $-52\pm 7.3\%$ ), and Kiattut Sermiat ( $-57.6\pm 14.2\%$ ). Measured  $\text{CO}_2$  concentrations (Fig. 3g) are consistently supersaturated with respect to atmospheric concentrations for sub-Isunnguata ( $685\pm 230$  ppm or  $58\pm 18$   $\mu\text{M}$ ), near atmospheric equilibrium for Russell ( $442\pm 31$  ppm or  $29\pm 4$   $\mu\text{M}$ ) and undersaturated for Kiattut Sermiat ( $263\pm 33$  ppm or  $19\pm 2$   $\mu\text{M}$ ). Mean  $\delta^{13}\text{C}-\text{CO}_2$  values (Fig. 3h) are lower in spring and fall for sub-Isunnguata ( $-16.6\pm 4.0\%$ ) compared to Russell ( $-13.7\pm 2.3\%$ ) and Kiattut Sermiat ( $-16.1\pm 1.6\%$ ) sites, though similar seasonal variation occurs for all sites with relatively more depleted values in the spring and fall compared to summer.

#### 3.2 Methane oxidation and relationship with discharge

Values of  $\epsilon_c$  are similar over time for sub-Isunnguata ( $38\pm 10\%$ ) and Russell ( $38\pm 9\%$ ) and are relatively higher in the summer sampling period, while Kiattut Sermiat  $\epsilon_c$  values are higher on average ( $42\pm 13\%$  with lowest values in the summer (Fig. 4a). Estimates of  $f_{\text{ox}}$  are similar between sub-Isunnguata ( $17\pm 15\%$ ), Russell ( $23\pm 15\%$ ), and Kiattut Sermiat sites ( $25\pm 22\%$ ; Fig. 4b). However,  $f_{\text{ox}}$  values are higher in the spring and fall sampling times compared to summer for sub-Isunnguata and Russell and approach 50% in the spring, while Kiattut Sermiat values decrease throughout the melt season.

$\text{CH}_4$  concentrations,  $\delta^{13}\text{C}-\text{CH}_4$  values, and  $f_{\text{ox}}$  are weakly negatively correlated to average daily discharge for both sub-Isunnguata and Russell sites (Fig. 5a, b and d), while  $\epsilon_c$  is weakly positively correlated with discharge for both sub-Isunnguata and Russell (Fig. 5c).

Deleted:

### 3.3 Mineral weathering impacts on CO<sub>2</sub> and relationship with discharge

Mineral weathering leads to net sequestration of CO<sub>2</sub> at all three sites (Fig. 6a). The magnitude of Net ΔCO<sub>2</sub> differs  
305 between sites with the lowest average values at sub-Isunnguata (-39±37 μM) followed by Russell (-65±32 μM) and Kiattut  
Sermiat (-98±17 μM) sites. Individual mineral weathering reactions produce differing contributions between sites and over  
time, with notable differences between southwest sites (sub-Isunnguata and Russell) and the southern Kiattut Sermiat site (Fig.  
6b). For instance, the proportional contribution of Carbs<sub>A</sub> is similar between sub-Isunnguata (17±11%) and Russell (15±6%),  
but lower at Kiattut Sermiat (8±1%; Fig. 6b). Kiattut Sermiat has a relatively greater contribution from Carb<sub>CA</sub> (62±2%)  
310 compared to sub-Isunnguata (41±10%) and Russell (38±6%), while Sil<sub>CA</sub> is lower at Kiattut Sermiat (28±1%) compared to  
sub-Isunnguata (41±17%), and Russell (47±11%). Kiattut Sermiat additionally exhibits low seasonal variability in the  
proportional contributions of individual mineral weathering reactions compared to sub-Isunnguata and Russell sites.

CO<sub>2-total</sub> represents CO<sub>2</sub> concentrations in the subglacial environment prior to addition and/or consumption of CO<sub>2</sub>  
through mineral weathering (Eq. 10; Fig. 7). Because the Net CO<sub>2-MW</sub> is always negative (more consumption than production),  
315 the value of CO<sub>2-total</sub> is always greater than measured concentrations (CO<sub>2-measured</sub>). Regardless of differences in CO<sub>2-measured</sub>  
between sites, the average CO<sub>2-total</sub> values are similar between sites and average 91±47 μM for sub-Isunnguata, 94±33 μM for  
Russell, and 117±16 μM for Kiattut Sermiat.

For both sub-Isunnguata and Russell sites, average daily discharge is negatively correlated with CO<sub>2</sub> concentrations  
(Fig. 8a), while positively correlated with δ<sup>13</sup>C-CO<sub>2</sub> (Fig. 8b).

320 Keeling plots between [CO<sub>2-total</sub>]<sup>-1</sup> and δ<sup>13</sup>C-CO<sub>2</sub> for each site indicate no linear relationship for Russell or Kiattut  
Sermiat samples, however a strong linear correlation is observed for sub-Isunnguata (r<sup>2</sup>=0.99; p<0.001) samples with the  
removal of one outlier, which also had the lowest CO<sub>2-total</sub> value (Fig 9).

## 4 Discussion

We observe orders of magnitude variability in dissolved CH<sub>4</sub> and CO<sub>2</sub> concentrations in subglacial discharge of the  
325 Greenland Ice Sheet, indicating significant differences in the magnitudes of the sources and sinks of these gases across time  
and space. Supersaturation of both CO<sub>2</sub> and CH<sub>4</sub> with respect to atmospheric concentrations indicates that sub-Isunnguata  
discharge is a source of both gases to the atmosphere, neighbouring Russell Glacier discharges water that is a source of CH<sub>4</sub>  
but near equilibrium with respect to CO<sub>2</sub>, while Kiattut Sermiat in southern Greenland is a sink of atmospheric CO<sub>2</sub> but near  
equilibrium with respect to CH<sub>4</sub> (Fig. 3e, g). Because CH<sub>4</sub> dynamics may be largely microbially driven while CO<sub>2</sub> dynamics  
330 include microbial as well as abiotic mineral weathering processes, we first discuss CH<sub>4</sub> dynamics including a comparison of  
concentrations, isotopic compositions, and extent of oxidation between sites and over the melt season. We then discuss CO<sub>2</sub>  
concentrations, impacts of mineral weathering reactions (Table 1), and an assessment of subglacial CO<sub>2</sub> sources, including

OM remineralization. These assessments will contribute to our understanding of the variability and controls of CH<sub>4</sub> and CO<sub>2</sub> concentrations in subglacial discharge from the Greenland Ice Sheet and may improve predictions of the impact of future ice melt on Arctic carbon budgets.

#### 4.1 Sources and sinks of CH<sub>4</sub>

Differences in CH<sub>4</sub> concentrations and relationships with discharge between sites imply heterogeneity in both the extent and controls of subglacial methanogenesis under the Greenland Ice Sheet. CH<sub>4</sub> supersaturation occurs at the two subglacial discharge sites that flow to the Akuliarusiarsuup Kuua (sub-Isunnguata and Russell), and concentrations are similar to the ranges reported in discharge of the Leverett Glacier (up to 600 nM; Lamarche-Gagnon et al., 2019), located near the Russell Glacier in this study (Fig. 2b). However, CH<sub>4</sub> concentrations are near atmospheric equilibrium for the Kiattut Sermiat site (Fig. 3e). Because methanogenesis is an anaerobic OM remineralization pathway, it is more likely to occur in subglacial environments isolated from atmospheric O<sub>2</sub> sources. Widespread observations of methanogenesis in glacial meltwater of southwest Greenland from this and other studies (Christiansen and Jørgensen, 2018; Dieser et al., 2014; Lamarche-Gagnon et al., 2019), and limited observations of CH<sub>4</sub> in subglacial discharge in southern Greenland, suggests heterogeneity in subglacial conditions that support methanogenesis. Methanogenesis fuelled by organic material overridden during ice sheet growth has been suggested as a potential climate feedback over glacial interglacial timescales (Wadham et al., 2008), and may contribute to observed variations in CH<sub>4</sub> concentrations.

Subglacial methane concentrations may additionally be controlled by hydrologic factors as the subglacial hydrological network develops throughout the melt season and channelization of meltwater conduits increases subglacial drainage efficiency (Andrews et al., 2015; Cowton et al., 2013). Drainage efficiency impacts both subglacial water residence time as well the transport of aerobic supraglacial meltwater to the ice bed. Both residence time and oxygen delivery may impact subglacial redox status and methanogenesis potential and favour methanogenesis when oxygen supply rates are low compared to OM remineralization rates. This condition is most likely to be met in distributed subglacial systems that are hydrologically isolated with limited inputs from aerobic supraglacial meltwater. Such a hydrologic control on methanogenesis is supported by the negative correlation between CH<sub>4</sub> concentrations and average daily discharge at both sites (Fig. 5a). This correlation would suggest that either CH<sub>4</sub> production occurs predominantly during periods of low discharge and greater residence time, or higher discharge results in the dilution of a CH<sub>4</sub>-laden subglacial water source. While both mechanisms would lead to a similar relationship between discharge and CH<sub>4</sub> concentrations, they carry different implications for subglacial methanogenesis. If limited by residence time, a hydrologic link between glacial hydrology and subglacial biogeochemistry would be established ~~because~~ supraglacial discharge ~~delivers~~ terminal electron acceptors to the ice bed ~~and would limit~~ ~~methanogenesis~~. If predominantly controlled by dilution, however, active methanogenesis would not be required; only the existence of meltwater pockets containing CH<sub>4</sub> that may or may not have been recently produced. Further discussion of these mechanisms is outside the scope of this study. While we have limited data to make further inferences about hydrologic controls

**Deleted:** due to the importance of

**Deleted:** for the delivery of

**Deleted:** for the active production of CH<sub>4</sub>

of methanogenesis, the presence of several outliers at the sub-Isunnguata site in particular (Fig. 5a) highlights the possibility for additional controls including stochastic drainage events or heterogeneity in subglacial CH<sub>4</sub> concentrations that result in variability in the relationship between concentration and discharge, as was observed in Lamarche-Gagnon et al. (2019).

Our results suggest heterogeneity in the extent of methanogenesis between outlet glaciers, but homogeneity of the microbial methanogenesis pathway as well as CH<sub>4</sub> oxidation dynamics between sites. Methanogenesis pathways may be evaluated by  $\delta^{13}\text{C-CH}_4$  as well as  $\epsilon_c$  values because they impart distinct  $\delta^{13}\text{C}$  signatures to CH<sub>4</sub> and CO<sub>2</sub> (Whiticar and Schoell, 1986). Dieser et al. (2014) measured a microbial  $\delta^{13}\text{C-CH}_4$  production signal at the Russell Glacier with values between -63‰ and -64‰, which was interpreted to reflect a possible combination of CH<sub>4</sub> produced through both acetoclastic and CO<sub>2</sub> reduction pathways. The most depleted  $\delta^{13}\text{C-CH}_4$  value measured at the sub-Isunnguata in this study was -62.7‰, close to values measured by Dieser et al. (2014) (Fig. 3f), and similar to values reported by Lamarche-Gagnon et al. (2019) for the Leverett Glacier. The similar isotopic ratio between our samples and that measured in active methanogenic communities could indicate that similar methanogenesis pathways occur across this region, or that the  $\delta^{13}\text{C-CH}_4$  of stored subglacial CH<sub>4</sub> has not been fractionated by oxidation or transport in the peak melt season when we observe these depleted  $\delta^{13}\text{C-CH}_4$  values.

While the exact contributions from each methanogenesis pathway cannot be inferred from isotopic information alone, the range of  $\epsilon_c$  values at outlet glaciers are consistent with predominantly acetoclastic methanogenesis during the peak melt season (Fig. 4a). However,  $\epsilon_c$  values fall below the expected range from acetoclastic methanogenesis during the early and late melt seasons and may result from variations in the extent of subglacial CH<sub>4</sub> oxidation. Seasonal variation in CH<sub>4</sub> oxidation is supported by consistency between  $\epsilon_c$  and  $f_{ox}$  values, which both indicate the greatest impact of oxidation (approaching 50%) in the early melt season compared to peak melt season (Fig. 4a, b), with additional evidence of elevated CH<sub>4</sub> oxidation in the late melt season at both sub-Isunnguata and Russell sites. Because our water sampling locations were slightly downstream of glacial discharge outlets, there is also the possibility that outgassing in between the outlet and our sampling location reduced dissolved CH<sub>4</sub> concentrations and led to more enriched isotopic compositions of remaining dissolved CH<sub>4</sub>. It is likely that some outgassing did occur, however it is unlikely that the extent of outgassing between the glacial outlet and our sampling location would vary significantly between sampling times, and thus outgassing would not fully explain temporal differences in concentration,  $\delta^{13}\text{C-CH}_4$ ,  $f_{ox}$ , or  $\epsilon_c$ . While our measured gas concentrations and isotopic compositions likely reflect some modification of CH<sub>4</sub> and CO<sub>2</sub> isotopic compositions due to outgassing, the differences over time are more likely due to changes in subglacial CH<sub>4</sub> dynamics than outgassing.

The extent of CH<sub>4</sub> oxidation may be controlled by multiple factors including oxygen availability, subglacial residence time, and subglacial hydrology, similar to methanogenesis. A hydrologic control of CH<sub>4</sub> oxidation is supported by relationships between  $f_{ox}$  and  $\epsilon_c$  with average daily discharge (collected at site AK4; Fig. 2b) at both sub-Isunnguata and Russell sites:  $f_{ox}$  is negatively related with discharge for both sites (Fig. 5b) while  $\epsilon_c$  is positively correlated with discharge (Fig. 5c). While weak, these correlations suggest that CH<sub>4</sub> oxidation is greatest during periods of low flow, which may be associated

Deleted: While our

Deleted: , they suggest

Deleted: suggests

Deleted: and additionally suggests

Deleted: CH<sub>4</sub> we measure in the sub-Isunnguata comes from active methanogenesis rather than old preserved

Deleted: reservoirs, at least

Deleted: While it

Deleted: These

with longer residence times to allow subglacial CH<sub>4</sub> oxidation, however this relationship could also result from differences in  
410 CH<sub>4</sub> sources throughout the melt season as the subglacial drainage network expands. Assuming the former, the delivery of  
oxygen to the subsurface by supraglacial melting does not appear to be a limiting factor in subglacial CH<sub>4</sub> oxidation, which  
should increase  $f_{ox}$  as more oxygenated supraglacial water is delivered to the subglacial system. Instead, the observed greater  
CH<sub>4</sub> oxidation during periods of low discharge may reflect mixing of methane-rich subglacial meltwater pockets and aerobic  
subglacial meltwater leading to CH<sub>4</sub> oxidation. Longer transit times during periods of low flow may allow more subglacial  
415 methane oxidation to occur than during peak discharge, when the development of channelized flow paths reduces meltwater  
residence time in the subglacial environment.

Our results indicate a high degree of heterogeneity in subglacial methanogenesis under the Greenland Ice Sheet, as  
well as a significant impact of CH<sub>4</sub> oxidation, which serves to reduce atmospheric CH<sub>4</sub> fluxes. Given the observed spatial and  
temporal heterogeneity of CH<sub>4</sub> concentrations and processes, further investigation of the spatial variability in outlet glacier  
420 CH<sub>4</sub> concentrations is needed to determine the impact of Greenland Ice Sheet loss on Arctic and global CH<sub>4</sub> budgets, while a  
better understanding of the controls of these differences will improve models of how CH<sub>4</sub> fluxes from subglacial discharge  
will change with continued warming.

#### 4.2 Sources and sinks of CO<sub>2</sub>

Dissolved CO<sub>2</sub> concentrations in subglacial discharge are consistently supersaturated with respect to atmospheric  
425 concentrations at the sub-Isunnguata site, near atmospheric equilibrium at the Russell Glacier, and undersaturated at Kiattut  
Sermiat, indicating that glacial meltwater from the Greenland Ice Sheet can serve as either a source or sink of CO<sub>2</sub> to the  
atmosphere. Similar to CH<sub>4</sub>, differences in dissolved CO<sub>2</sub> dynamics (Fig. 3g) imply variability in carbon processes under the  
Greenland Ice Sheet. We first discuss potential subglacial CO<sub>2</sub> sources, including OM remineralization, followed by a  
discussion of CO<sub>2</sub> consumption due to mineral weathering.

##### 430 4.2.1 Subglacial CO<sub>2</sub> sources

There are many potential sources of CO<sub>2</sub> in the subglacial environment including dissolution of atmospheric gases in  
air-filled conduits or fractures in ice, CO<sub>2</sub> contained in ice bubbles (Fig. 1; Anklin et al., 1995; Graly et al., 2017) mechanical  
grinding and volatilization of fluid inclusions in bedrock (Macdonald et al., 2018), and OM remineralization. While previous  
studies have indicated that additional atmospheric CO<sub>2</sub> input through fractures and air-filled conduits may supply sufficient  
435 CO<sub>2</sub> to drive mineral weathering observed in many subglacial environments, including several sites in Greenland (Graly et al.,  
2017), CO<sub>2</sub> is also a product of OM remineralization, which is believed to account for CH<sub>4</sub> concentrations elevated above  
atmospheric equilibrium at the two southwest sites in this study. Both CO<sub>2</sub> and CH<sub>4</sub> exhibit negative correlations with average  
daily discharge for both sub-Isunnguata and Russell sites, and could suggest a common OM remineralization source (Fig. 8a).  
While the magnitude of this source and its relative importance compared to other subglacial CO<sub>2</sub> sources is currently unknown,

Deleted: Glacier

differing sources of carbonic acid for mineral weathering reactions carry different implications for subglacial CO<sub>2</sub> budgets. For instance, carbonic acid weathering driven by invasion of atmospheric CO<sub>2</sub> would represent a sink of atmospheric CO<sub>2</sub>, but carbonic acid weathering driven by OM remineralization would instead serve to consume CO<sub>2</sub> from *in situ* sources and limit the potential for subglacial meltwater to be an atmospheric CO<sub>2</sub> source once discharged from the glacier. Determining the sources of carbonic acid to subglacial weathering reactions is therefore critical to understand the controls of mineral weathering in subglacial environments and its role in atmospheric CO<sub>2</sub> sequestration.

Comparisons between measured  $\delta^{13}\text{C-CO}_2$  in subglacial discharge samples and likely  $\delta^{13}\text{C-CO}_2$  values of CO<sub>2</sub> sources indicate that CO<sub>2</sub> sources differ between sites, with OM remineralization as the most important CO<sub>2</sub> source at the sub-Isunnguata but likely not the predominant or sole source at Russell or Kiattut Sermiat glaciers. Keeling plots of  $[\text{CO}_{2\text{-total}}]^{-1}$  versus  $\delta^{13}\text{C-CO}_2$  indicate that CO<sub>2-total</sub> may be represented by a two-end member mixing model for sub-Isunnguata discharge, but not for discharge from the Russell and Kiattut Sermiat glaciers (Fig. 9). Mixing model end members include a <sup>13</sup>C-enriched, lower concentration CO<sub>2</sub> source and a <sup>13</sup>C-depleted, higher concentration CO<sub>2</sub> source. The y-intercept of the regression between  $[\text{CO}_{2\text{-total}}]^{-1}$  versus  $\delta^{13}\text{C-CO}_2$ , which represents the isotopic signature of the high-CO<sub>2</sub> endmember, is -27.4‰. This value is close to what would be expected from OM remineralization as indicated by remineralized OM in Greenlandic heath soils that produced  $\delta^{13}\text{C-CO}_2$  of approximately -27 to -25‰ (Ravn et al., 2020), and thawed Alaskan permafrost soils that produced  $\delta^{13}\text{C-CO}_2$  of between -20 to -30‰ for (Mauritz et al., 2019), both of which may be similar to subglacial organic matter. The low-CO<sub>2</sub> end member could reflect atmospheric CO<sub>2</sub> input, with an associated  $\delta^{13}\text{C-CO}_2$  value of approximately -8‰. While the  $\delta^{13}\text{C-CO}_2$  value of the lowest-CO<sub>2-total</sub> samples in the sub-Isunnguata Keeling plot (e.g. highest  $[\text{CO}_{2\text{-total}}]^{-1}$  not including the outlier) is slightly depleted compared to atmospheric values at -12.1‰, even the lowest CO<sub>2</sub> concentrations measured at sub-Isunnguata are supersaturated with respect to atmospheric concentrations (Fig. 3g). ~~Consistent CO<sub>2</sub> supersaturation suggests~~ that OM remineralization contributes CO<sub>2</sub> even for low CO<sub>2</sub>-concentration samples and isotopically depletes the subglacial CO<sub>2</sub> reservoir.

While  $\delta^{13}\text{C-CO}_2$  values of Russell and Kiattut Sermiat samples are within the range of sub-Isunnguata samples, suggesting possible contributions of CO<sub>2-atm</sub> and CO<sub>2-OM</sub>, scatter in the Keeling plots indicate variability in the CO<sub>2</sub> concentration and/or isotopic composition of end members, or significant contributions of at least one other major subglacial CO<sub>2</sub> source. We address both possibilities here. While atmospheric CO<sub>2</sub> concentrations and  $\delta^{13}\text{C}$  values should be relatively invariable, CO<sub>2-OM</sub> may vary both in concentration and isotopic composition, depending on variability in the quantity and composition of organic deposits as well as remineralization rates. For instance, if remineralization largely occurs in hydrologically isolated subglacial meltwater pockets, some variability in the concentration and  $\delta^{13}\text{C-CO}_2$  of CO<sub>2-OM</sub> is likely. While no data yet exist to characterize the variability in subglacial OM reservoirs, variability in either concentration or isotopic composition of CO<sub>2-OM</sub> could plausibly result in the scatter shown in Figure 9. Additional subglacial CO<sub>2</sub> sources from ice bubbles, or lithogenic CO<sub>2</sub> liberated by mechanical grinding would be expected to enrich rather than deplete the  $\delta^{13}\text{C-CO}_2$

**Deleted:** ‰; however,

**Deleted:** Thereby suggesting

475 values of the samples relative to modern atmospheric  $\delta^{13}\text{C}$ - $\text{CO}_2$  values. Ice bubbles contain gaseous  $\text{CO}_2$  at concentrations and  
isotopic compositions reflecting atmospheric conditions during ice formation. While heterogeneity may result from gas  
bubbles recording changes in atmospheric  $\text{CO}_2$ , variability in  $\delta^{13}\text{C}$ - $\text{CO}_2$  of gas bubble  $\text{CO}_2$  should be only a few per mil, which  
is small compared to the variation observed in Russell and Kiattut Sermiat samples (e.g., Tipple et al., 2010; Fig. 9). Gas  
bubble  $\text{CO}_2$  should also be  $^{13}\text{C}$ -enriched compared to modern atmospheric  $\text{CO}_2$  due to fossil fuel contributions, and thus would  
480 be unlikely to cause the observed depletion of  $^{13}\text{C}$  in the subglacial water.

Recent work has also highlighted the potential for subglacial mechanical grinding to result in  $\text{CO}_2$  production through  
the volatilization of bedrock fluid inclusions (Macdonald et al., 2018). While this process was found to produce sufficient  $\text{CO}_2$   
to drive approximately 20% of mineral weathering in Svalbard subglacial environments, the expected isotopic composition of  
lithogenic  $\text{CO}_2$  is more  $^{13}\text{C}$ -enriched than our measured  $\delta^{13}\text{C}$ - $\text{CO}_2$  values. For instance, estimates of  $\delta^{13}\text{C}$  for bulk hydrocarbons  
485 in fluid inclusions in the Ilimaussaq alkaline complex of South Greenland have values of  $-4.5 \pm 1.5\text{‰}$  (Madsen, 2001), which  
is close to the  $\delta^{13}\text{C}$ - $\text{CO}_2$  of  $\text{CO}_2$  in fluid inclusions in the Bamble granulite sector of South Norway ( $\sim -6\text{‰}$ ; Newton et al.,  
1980). Because mechanical grinding should not fractionate the  $\delta^{13}\text{C}$ - $\text{CO}_2$  values (Lüders et al., 2012), our low  $\delta^{13}\text{C}$ - $\text{CO}_2$  values  
suggest this source is small relative to other sources.

One additional source or sink of  $\text{CO}_2$  to some of our samples is atmospheric exchange as water flows from the  
490 subglacial outlet site to our sampling sites. However, atmospheric  $\text{CO}_2$  exchange after discharge would have the same impact  
on Keeling plots as atmospheric  $\text{CO}_2$  exchange prior to discharge. Incorporation of an atmospheric source between the outlet  
and sample site would be most likely at Kiattut Sermiat where  $\text{CO}_2$  concentrations are undersaturated with respect to  
atmospheric concentrations, which would promote invasion of atmospheric  $\text{CO}_2$ . However, the measured  $\delta^{13}\text{C}$ - $\text{CO}_2$  values are  
more  $^{13}\text{C}$ -depleted than modern atmospheric  $\text{CO}_2$  and are not consistent with atmospheric  $\text{CO}_2$  as the sole or dominant source  
495 of  $\text{CO}_2$  to these samples (Fig. 9).

While more information is needed to determine all possible sources of  $\text{CO}_2$  to Russell and Kiattut Sermiat samples,  
 $\delta^{13}\text{C}$ - $\text{CO}_2$  values of samples from both sites imply mixing between a  $^{13}\text{C}$ -depleted  $\text{CO}_2$  source, such as OM remineralization,  
and one or more  $^{13}\text{C}$ -enriched  $\text{CO}_2$  sources, such as atmospheric or lithogenic  $\text{CO}_2$ . Similar to  $\text{CH}_4$ , concentrations and isotopic  
compositions of gases may be impacted by atmospheric exchange between the glacial outlet and our sampling locations, which  
500 would alter dissolved  $\text{CO}_2$  concentrations and  $\delta^{13}\text{C}$ - $\text{CO}_2$  compositions to values more similar to atmospheric values. Therefore,  
we are unable to distinguish the impacts of atmospheric exchange that occurs prior to discharge from exchange that occurs  
between discharge and our sampling locations. However, the impact of this exchange should be relatively constant between  
sampling times and sampling locations, therefore outgassing would not account for temporal or spatial variability in  $\text{CO}_2$   
concentrations or isotopic compositions between sites.

#### 505 4.2.2 Subglacial CO<sub>2</sub> sink: mineral weathering reactions

Mineral weathering leads to net CO<sub>2</sub> consumption in all subglacial discharge samples (Fig. 6), and thus the measured CO<sub>2</sub> concentrations at glacial outlets represent only a fraction of the total CO<sub>2</sub> that would have been present in the absence of mineral weathering reactions (CO<sub>2-total</sub>; Eq. 10). Net consumption occurs because the CO<sub>2</sub> source from Carb<sub>SA</sub> is ubiquitously low compared to sinks from either Carb<sub>CA</sub> or Sil<sub>CA</sub> (Fig. 6b). The range in Net CO<sub>2-MW</sub> is similar between subglacial discharge sites (between 10-150 μM; Fig. 6a), but average values increase from Kiattut Sermiat to Russell to sub-Isunnguata, likely reflecting the relative weatherability of alkaline igneous rocks, granulite facies gneisses, and amphibolite facies gneisses. Kiattut Sermiat is characterized by a relatively high proportion of Carb<sub>CA</sub> compared to sub-Isunnguata and Russell sites, which may arise from the presence of trace carbonates in abundant and readily weatherable basaltic intrusions as has been implicated in other studies (Urta et al., 2019). The relatively greater influence of carbonate dissolution compared to silicate dissolution on Total CO<sub>2-MW</sub> at Kiattut Sermiat may also relate to more rapid dissolution kinetics of carbonates, which allow carbonate dissolution to have a large influence on major cation and anion load even when carbonates are only present in trace amounts (Deuerling et al., 2019; Tranter, 2005). At sub-Isunnguata and Russell sites, Sil<sub>CA</sub> has a greater influence than Carb<sub>CA</sub> on Total CO<sub>2-MW</sub>, which could result from either a lower abundance of trace carbonates to participate in weathering reactions, or relatively longer subglacial residence times that would allow a greater accumulation of silicate weathering products.

520 Despite the impact of Carb<sub>CA</sub> on Total CO<sub>2-MW</sub> at Kiattut Sermiat compared to sub-Isunnguata and Russell sites, Carb<sub>SA</sub> is notably lower at Kiattut Sermiat than other sites and suggests a limited role for sulfuric acid weathering that may relate to subglacial sulfide oxidation dynamics. Lower abundances of sulfide minerals in the subglacial environment may limit the production of sulfuric acid, and could result from differences in lithology between sites, the depletion of sulfide minerals due to prior weathering (Graly et al., 2014), or weathering occurring in anoxic environments that limit the oxidation of sulfide to sulfuric acid (Deuerling et al., 2019). ~~The kinetics of sulfide oxidation may also significantly differ between sites depending on the relative contributions of abiotic compared to microbially mediated sulfide oxidation, as microbially mediated sulfide oxidation is several orders of magnitude faster than abiotic sulfide oxidation (Boyd et al., 2014; Harrold et al., 2016). Rapid microbially mediated sulfide oxidation has been implicated in the development of anaerobic conditions, which could also support subglacial methanogenesis (Sharp et al., 1999; Stibal et al., 2012; Wadham et al., 2010). Observations of higher CH<sub>4</sub> concentrations as well as higher contributions of Carb<sub>SA</sub> at sub-Isunnguata and Russell compared to Kiattut Sermiat may therefore be linked to subglacial microbial activity, which is known to vary based on factors such as the presence of organic and fine-grained rock flour to serve as growth substrates, insulation from fluctuations in temperature, and delivery of nutrients and organic matter from supraglacial sources (Sharp et al., 1999). If microbially driven, our results suggest possible linkages between microbial processes and subglacial mineral weathering regimes, with significant impacts to both CH<sub>4</sub> and CO<sub>2</sub> dynamics due to the role of Carb<sub>SA</sub> as a CO<sub>2</sub> source (Table 1).~~

530

535

**Deleted:** The kinetics of sulfide oxidation may also significantly differ between sites depending on the relative contributions of abiotic compared to microbially mediated sulfide oxidation, as microbially mediated sulfide oxidation is several orders of magnitude faster than abiotic sulfide oxidation.

**Deleted:** (Sharp et al., 1999).

Whether controlled by geochemical, microbial, or mechanical processes, the relationships between CO<sub>2</sub> concentrations and δ<sup>13</sup>C-CO<sub>2</sub> and average daily discharge are similar between sub-Isunnguata and Russell sites (Fig. 8). These



545 similarities suggest that underlying controls in carbonate chemistry may be consistent between sites despite the heterogeneity  
in measured dissolved CO<sub>2</sub> concentrations. For both sub-Isunnguata and Russell sites, mineral weathering reactions consume  
CO<sub>2</sub>, which implies contributions from *in situ* CO<sub>2</sub> sources (such as atmospheric CO<sub>2</sub> invasion or OM remineralization) to  
produce measured CO<sub>2</sub> concentrations. The different CO<sub>2</sub> concentrations observed between sites therefore appear to result  
550 from the strength of *in situ* CO<sub>2</sub> sources relative to CO<sub>2-MW</sub>, both of which impart the greatest chemical change at times of low  
discharge and high subglacial residence time. At Kiattut Sermiat, where measured CO<sub>2</sub> concentrations are lowest, the  
magnitude of *in situ* sources is insufficient to maintain atmospheric equilibrium, leading subglacial discharge to be a sink of  
atmospheric CO<sub>2</sub>, while CO<sub>2-total</sub> maintains close to atmospheric equilibrium concentrations at the Russell Glacier. At sub-  
Isunnguata, however, OM remineralization produces more CO<sub>2</sub> than is consumed by mineral weathering and causes meltwater  
to be a source of CO<sub>2</sub> to the atmosphere. This finding implies that subglacial mineral weathering serves to partially or fully  
555 consume CO<sub>2</sub> produced from *in situ* sources under the Greenland Ice Sheet but does not always serve to directly consume  
modern atmospheric CO<sub>2</sub>.

## 5 Conclusions

Subglacial reactions impact the concentrations of CO<sub>2</sub> and CH<sub>4</sub> in subglacial discharge of Greenland Ice Sheet, and  
differences in the relative magnitudes of microbial and geochemical processes result in a high degree of previously  
unrecognized heterogeneity between glacial discharge sites of the Greenland Ice Sheet. Our results imply a significant role of  
560 OM remineralization in driving this heterogeneity and leading to CO<sub>2</sub> and CH<sub>4</sub> supersaturation at the sub-Isunnguata site, and  
CH<sub>4</sub> supersaturation at the Russell site. Heterogeneity may result in significant uncertainty in total greenhouse gas flux  
estimates from subglacial systems of the Greenland Ice Sheet, which will be an increasingly important carbon flux as the Arctic  
warms in the coming decades. While heterogeneous, the uncertainty in greenhouse gas fluxes from Greenland Ice Sheet  
meltwater may be reduced by a better understanding of the controls and variability of the weathering reactions and microbial  
565 processes driving heterogeneous gas concentrations. Such a process-based understanding could also improve estimates of the  
impact of greenhouse gas variability associated with the growth and retreat of continental ice sheets on over glacial-interglacial  
timescales. Subglacial OM remineralization further implies the existence of links between subglacial OM deposits and export  
of other biogeochemical solutes from the Greenland Ice Sheet, including nutrients as well as redox-sensitive elements. While  
the export of nutrients from the Greenland Ice Sheet has been the focus of numerous studies (Bhatia et al., 2013; Hawkings et  
570 al., 2016; Lawson et al., 2014), little is currently known regarding the role of OM sources in governing these exports. Given  
the variability in greenhouse gas concentrations observed in this study, constraining the extent of heterogeneity in outlet  
glaciers of the Greenland Ice Sheet as well as the biogeochemical, hydrologic, and geologic controls of this heterogeneity will  
be important for upscaling atmospheric fluxes as well as efforts to predict impacts of ice loss on carbon and nutrient budgets  
due to current and future melting of the Greenland Ice Sheet.

## 575 **Author Contribution**

Jonathan B. Martin and Ellen E. Martin participated in conceptualization, data collection, data interpretation, reviewing and editing the manuscript, and acquired the funding for this project. Asa Rennermalm provided the discharge data that was used in analyses of discharge-concentration relationships. Shaily Rahman participated in data collection and early interpretation and presentation of results. Andrea J. Pain participated in conceptualization, data collection, analysis, and interpretation, and took the lead on writing the manuscript with contributions from Jonathan B. Martin, Ellen E. Martin, and Asa Rennermalm.

## **Acknowledgements**

We acknowledge the members of our field teams: Daniel Fischer, Fabio Da Prat, Hailey Hall, Mark Robbins, Scott Schnur, and Michelle D. Kisbye. Additional invaluable support was provided by Steven DiEgidio, Nini Frydkjær Brandt, Inga Gisladottir, and Jacky Simoud. We are grateful for the excellent field support provided by the Kangerlussuaq International Science Station and Polar Field Services (CH2M Hill). This work was funded by the National Science Foundation grant (ANS-1603452). The authors declare that they have no conflict of interest. Data is accessible on the Arctic Data Center (doi:10.18739/A2F76672G) including gas and nutrient data (<https://cn.dataone.org/cn/v2/resolve/urn:uuid:c1051a07-cbdf-4061-ae44-c1472f61e3fe>) and major element concentrations used for geochemical modeling (<https://cn.dataone.org/cn/v2/resolve/urn:uuid:65d272f6-d280-4fcc-8aaa-4805f12ca6ae>). We are grateful to Marek Stibal and an anonymous reviewer who made suggestions that greatly improved the manuscript, as well as Joseph Graly for assistance improving the accuracy of presented geographical locations.

## **References**

- Andrews, L. C., Catania, G. A., Hoffman, M. J., Gulley, J. D., Lüthi, M. P., Ryser, C., Hawley, R. L. and Neumann, T. A.: Direct observations of evolving subglacial drainage beneath the Greenland Ice Sheet, *Nature*, 514(7520), 80–83, doi:10.1038/nature13796, 2015.
- Anklin, M., Barnola, J. M., Schwander, J., Stauffer, B. and Raynaud, D.: Processes affecting the CO<sub>2</sub> concentrations measured in Greenland ice, *Tellus B*, 47(4), 461–470, doi:10.1034/j.1600-0889.47.issue4.6.x, 1995.
- van As, D., Hasholt, B., Ahlstrøm, A. P., Box, J. E., Cappelen, J., Colgan, W., Fausto, R. S., Mernild, S. H., Bech, A., Noël, B. P. Y., Petersen, D. and van Den Broeke, M. R.: Reconstructing Greenland Ice Sheet meltwater discharge through the Watson River (1949–2017), *Arctic, Antarct. Alp. Res.*, 50(1), doi:10.1080/15230430.2018.1433799, 2018.
- Van As, D., Mikkelsen, A. B., Nielsen, M. H., Box, J. E., Liljedahl, L. C., Lindbäck, K., Pitcher, L. and Hasholt, B.: Hypsometric amplification and routing moderation of Greenland ice sheet meltwater release, *Cryosphere*, 11(3), 1371–1386, doi:10.5194/tc-11-1371-2017, 2017.

- As, D. Van, Hasholt, B., Ahlstrøm, A. P., Box, J. E., Cappelen, J., Colgan, W., Fausto, R. S., Mernild, S. H., Bech, A., Noël,  
605 B. P. Y., Petersen, D., Broeke, M. R. Van Den, As, D. Van, Hasholt, B., Ahlstrøm, A. P., Box, J. E., Colgan, W., Fausto, R.  
S., Mernild, S. H. and Mikkelsen, A. B.: Reconstructing Greenland Ice Sheet meltwater discharge through the Watson River (1949 – 2017) Reconstructing Greenland Ice Sheet meltwater discharge through the Watson, Arctic, Antarct. Alp. Res., 50(1),  
doi:10.1080/15230430.2018.1433799, 2018.
- Berner, R. A., Lasaga, A. C. and Garrels, R. M.: The carbonate-silicate geochemical cycle and its effect on atmospheric carbon  
610 dioxide over the past 100 million years., Am. J. Sci., 283(7), 641–683, doi:10.2475/ajs.283.7.641, 1983.
- Bhatia, M. P., Kujawinski, E. B., Das, S. B., Breier, C. F., Henderson, P. B. and Charette, M. A.: Greenland meltwater as a  
significant and potentially bioavailable source of iron to the ocean, Nat. Geosci., 6(4), 274–278, doi:10.1038/ngeo1746, 2013.
- [Boyd, E. S., Hamilton, T. L., Havig, J. R., Skidmore, M. L. and Shock, E. L.: Chemolithotrophic primary production in a  
subglacial ecosystem, Appl. Environ. Microbiol., 80\(19\), 6146–6153, doi:10.1128/AEM.01956-14, 2014.](#)
- 615 Christiansen, J. R. and Jørgensen, C. J.: First observation of direct methane emission to the atmosphere from the subglacial  
domain of the Greenland Ice Sheet, Sci. Rep., 8(1), 2–7, doi:10.1038/s41598-018-35054-7, 2018.
- Cowton, T., Nienow, P., Sole, A., Wadham, J., Lis, G., Bartholomew, I., Mair, D. and Chandler, D.: Evolution of drainage  
system morphology at a land - terminating Greenlandic outlet glacier, , 118, 29–41, doi:10.1029/2012JF002540, 2013.
- Deuerling, K. M., Martin, J. B., Martin, E. E. and Scribner, C. A.: Hydrologic exchange and chemical weathering in a proglacial  
620 watershed near Kangerlussuaq, west Greenland, J. Hydrol., 556, 220–232, doi:10.1016/j.jhydrol.2017.11.002, 2018.
- Deuerling, K. M., Martin, J. B., Martin, E. E., Abermann, J., Myreng, S. M., Petersen, D. and Rennermalm, A. K.: Chemical  
weathering across the western foreland of the Greenland Ice Sheet, Geochim. Cosmochim. Acta, 245(245), 426–440,  
doi:10.1016/j.gca.2018.11.025, 2019.
- Dieser, M., Broemsen, E. L. J. E., Cameron, K. A., King, G. M., Achberger, A., Choquette, K., Hagedorn, B., Sletten, R.,  
625 Junge, K. and Christner, B. C.: Molecular and biogeochemical evidence for methane cycling beneath the western margin of  
the Greenland Ice Sheet, ISME J., 8(11), 2305–2316, doi:10.1038/ismej.2014.59, 2014.
- van Gool, J. A., Alsop, G. I., Arting, U. E., Garde, A. A., Knudsen, C., Krawiec, A. W., Mazur, S., Nygaard, J., Piazzolo, S.  
and Thomas, C. W.: Precambrian geology of the northern Nagssugtoqidian orogen, West Greenland: mapping in the  
Kangaatsiaq area, Geol. Greenl. Surv. Bull., 191, 13–23, 2002.
- 630 Graly, J., Harrington, J. and Humphrey, N.: Combined diurnal variations of discharge and hydrochemistry of the Isunnguata  
Sermia outlet, Greenland Ice Sheet, Cryosphere, 11(3), 1131–1140, doi:10.5194/tc-11-1131-2017, 2017a.
- Graly, J. A., Humphrey, N. F., Landowski, C. M. and Harper, J. T.: Chemical weathering under the Greenland Ice Sheet,  
Geology, 551–554, doi:10.1130/G35370.1, 2014.

635 Graly, J. A., Drever, J. I. and Humphrey, N. F.: Calculating the balance between atmospheric CO<sub>2</sub> drawdown and organic carbon oxidation in subglacial hydrochemical systems, *Global Biogeochem. Cycles*, 31(4), 709–727, doi:10.1002/2016GB005425, 2017b.

[Harrold, Z. R., Skidmore, M. L., Hamilton, T. L., Desch, L., Amada, K., Van Gelder, W., Glover, K., Roden, E. E. and Boyd, E. S.: Aerobic and anaerobic thiosulfate oxidation by a cold-adapted, subglacial chemoautotroph, \*Appl. Environ. Microbiol.\*, 82\(5\), 1486–1495, doi:10.1128/AEM.03398-15, 2016.](#)

640 Hasholt, B., As, D. Van, Mikkelsen, A. B., Mernild, S. H., Yde, J. C., Hasholt, B., As, D. Van, Mikkelsen, A. B., Mernild, S. H. and Hasholt, B.: Observed sediment and solute transport from the Kangerlussuaq sector of the Greenland Ice Sheet (2006–2016), *Arctic, Antarct. Alp. Res.*, 50(1), doi:10.1080/15230430.2018.1433789, 2018.

Hawkings, J., Wadham, J., Tranter, M., Telling, J. and Bagshaw, E.: The Greenland Ice Sheet as a hot spot of phosphorus weathering and export in the Arctic, *Global Biogeochem. Cycles*, 191–210, doi:10.1002/2015GB005237, Received, 2016.

645 Henriksen, N., Higgins, A. K., Kalsbeek, F. and Pulvertaft, T. C. R.: Greenland from Archaean to Quaternary. Descriptive text to the 1995 Geological map of Greenland, 1:2 500 000. 2nd edition, *GEUS Bull.*, 18(SE-MONOGRAPH), 1–126, doi:10.34194/geusb.v18.4993, 2009.

Hersch, R.: *Hydrometry*, 2nd Edition., John Wiley & Sons, Ltd., Chichester, New York, Weinheim, Brisbane, Singapore, Toronto., 1999.

650 Hindshaw, R. S., Rickli, J., Leuthold, J., Wadham, J. and Bourdon, B.: Identifying weathering sources and processes in an outlet glacier of the Greenland Ice Sheet using Ca and Sr isotope ratios, *Geochim. Cosmochim. Acta*, 145, 50–71, doi:10.1016/j.gca.2014.09.016, 2014.

[Kalsbeek, F. and Taylor, P. N.: Isotopic and chemical variation in granites across a Proterozoic continental margin- the Ketilidian mobile belt of South Greenland, \*Earth Planet. Sci. Lett.\*, 73\(1\), 65–80, 1985.](#)

655 Keeling, C. D.: The concentration and isotopic abundances of atmospheric carbon dioxide in rural areas, *Geochim. Cosmochim. Acta*, 13(4), 322–334, doi:10.1016/0016-7037(58)90033-4, 1958.

Lamarche-Gagnon, G., Wadham, J. ., Sherwood Lollar, B., Arndt, S., Fietzek, P., Beaton, A. D., Tedstone, A. J., Telling, J., Bagshaw, E. A., Hawkings, J. R., Kohler, T. J., Zarsky, J. D., Mowlem, M. C., Anesio, A. M. and Stibal, M.: Greenland melt drives continuous export of methane from the ice-sheet bed, *Nature*, 565(7737), 73–77, doi:http://dx.doi.org/10.1038/s41586-660 018-0800-0, 2019.

Larsen, N. K., Find, J., Kristensen, A., Bjørk, A. A., Kjeldsen, K. K., Odgaard, B. V., Olsen, J. and Kjær, K. H.: Holocene ice marginal fluctuations of the Qassimiut lobe in South Greenland, *Nat. Publ. Gr.*, 1–11, doi:10.1038/srep22362, 2016.

Lawson, E. C., Wadham, J. L., Tranter, M., Stibal, M., Lis, G. P., Butler, C. E. H., Laybourn-Parry, J., Nienow, P., Chandler,

**Deleted:** ISO Guide 98-3 (2008), Guide 98-3. Uncertainty of measurement - Part 3: Guide to the expression of uncertainty in measurement (GUM:1995), Guid. 98-3, (148902), 130, doi:10.1373/clinchem.2003.030528.

- D. and Dewsbury, P.: Greenland ice sheet exports labile organic carbon to the arctic oceans, *Biogeosciences*, 11(14), 4015–4028, doi:10.5194/bg-11-4015-2014, 2014.
- 670 Lindbäck, K., Pettersson, R., Hubbard, A. L., Doyle, S. H., As, D., Mikkelsen, A. B. and Fitzpatrick, A. A.: Subglacial water drainage, storage, and piracy beneath the Greenland ice sheet, , 7606–7614, doi:10.1002/2015GL065393. Received, 2015.
- Lüders, V., Plessen, B. and di Primio, R.: Stable carbon isotopic ratios of CH<sub>4</sub>-CO<sub>2</sub>-bearing fluid inclusions in fracture-fill mineralization from the Lower Saxony Basin (Germany) - A tool for tracing gas sources and maturity, *Mar. Pet. Geol.*, 30(1), 174–183, doi:10.1016/j.marpetgeo.2011.10.006, 2012.
- 675 Ludwig, W., Amiotte Suchet, P. and Probst, J.-L.: Enhanced chemical weathering of rocks during the last glacial maximum: a sink for atmospheric CO<sub>2</sub>?, *Chem. Geol.*, 159, 147–161 [online] Available from: <http://www.sciencedirect.com/science/article/pii/S0009254199000388> Cnpapers2://publication/uuid/9F3040A1-7901-480E-B435-BA665074AC32, 1999.
- Macdonald, M. L., Wadham, J. L., Telling, J. and Skidmore, M. L.: Glacial Erosion Liberates Lithologic Energy Sources for Microbes and Acidity for Chemical Weathering Beneath Glaciers and Ice Sheets, *Front. Earth Sci.*, 6(November), 1–15, doi:10.3389/feart.2018.00212, 2018.
- Madsen, J. K.: A review of the composition and evolution of hydrocarbon gases during solidification of the Ilimaussaq alkaline complex, South Greenland, *Geol. Greenl. Surv. Bull.*, 190, 159–166, 2001.
- Mahieu, K., De Visscher, A., Vanrolleghem, P. A. and Van Cleemput, O.: Modelling of stable isotope fractionation by methane oxidation and diffusion in landfill cover soils, *Waste Manag.*, 28(9), 1535–1542, doi:10.1016/j.wasman.2007.06.003, 2008.
- 685 Mauritz, M., Celis, G., Ebert, C., Hutchings, J., Ledman, J., Natali, S. M., Pegoraro, E., Salmon, V. G., Schädel, C., Taylor, M. and Schuur, E. A. G.: Using Stable Carbon Isotopes of Seasonal Ecosystem Respiration to Determine Permafrost Carbon Loss, *J. Geophys. Res. Biogeosciences*, 124(1), 46–60, doi:10.1029/2018JG004619, 2019.
- Mouginot, J., Rignot, E., Björk, A. A., van den Broeke, M., Millan, R., Morlighem, M., Noël, B., Scheuchl, B. and Wood, M.: 690 Forty-six years of Greenland Ice Sheet mass balance from 1972 to 2018, *Proc. Natl. Acad. Sci.*, 116(19), 201904242, doi:10.1073/pnas.1904242116, 2019.
- Myrntinen, A., Becker, V. and Barth, J. A. C.: A review of methods used for equilibrium isotope fractionation investigations between dissolved inorganic carbon and CO<sub>2</sub>, *Earth-Science Rev.*, 115(3), 192–199, doi:10.1016/j.earscirev.2012.08.004, 2012.
- 695 Newton, R. C., Smith, J. V. and Windley, B. F.: Carbonic metamorphism, granulites and crustal growth, *Nature*, 288(5786), 45–50, doi:10.1038/288045a0, 1980.

[Organization\), W. \(World M.: Manual on Stream Gauging. Volume I: Fieldwork, 2010.](#)

**Deleted:** Musilova, M., Tranter, M., Wadham, J., Telling, J., Tedstone, A. and Anesio, A. M.: Microbially driven export of labile organic carbon from the Greenland ice sheet, *Nat. Geosci.*, 10(5), 360–365, doi:10.1038/ngco2920, 2017.

- Pain, A. J., Martin, J. B. and Young, C. R.: Sources and sinks of CO<sub>2</sub> and CH<sub>4</sub> in siliciclastic subterranean estuaries, *Limnol. Oceanogr.*, 64(4), 1500–1514, doi:10.1002/lno.11131, 2019.
- Parkhurst, L.: Geochemical mole-balance modeling with uncertain data, *Water Resour. Res.*, 33(8), 1957–1970, 1997.
- 705 Da Prat, F. A. and Martin, E.: Weathering in the Glacial Foreland of Southern and Western Greenland, *Univ. Florida J. Undergrad. Res.*, 20(2), doi:10.32473/ufjr.v20i2.106168, 2019.
- Preuss, I., Knoblauch, C., Gebert, J. and Pfeiffer, E. M.: Improved quantification of microbial CH<sub>4</sub> oxidation efficiency in arctic wetland soils using carbon isotope fractionation, *Biogeosciences*, 10(4), 2539–2552, doi:10.5194/bg-10-2539-2013, 2013.
- 710 Ravn, N. R., Elberling, B. and Michelsen, A.: Arctic soil carbon turnover controlled by experimental snow addition, summer warming and shrub removal, *Soil Biol. Biochem.*, 142(December 2019), 107698, doi:10.1016/j.soilbio.2019.107698, 2020.
- Rennermalm, A. K., Smith, L. C., Chu, V. W., Forster, R. R., Box, J. E. and Hagedorn, B.: Proglacial river stage, discharge, and temperature datasets from the Akuliarusiarsuup Kuua River northern tributary, Southwest Greenland, 2008–2011, *Earth Syst. Sci. Data Discuss.*, 2100(4), 1–12, doi:10.5194/essd-4-1-2012, 2012.
- 715 Rennermalm, A. K., Smith, L. C., Chu, V. W., Box, J. E., Forster, R. R., Broeke, M. R. Van Den and As, D. Van: Evidence of meltwater retention within the Greenland ice sheet, *Cryosph.*, 1433–1445, doi:10.5194/tc-7-1433-2013, 2013.
- Repo, M. E., Huttunen, J. T., Naumov, A. V., Chichulin, A. V., Lapshina, E. D., Bleuten, W. and Martikainen, P. J.: Release of CO<sub>2</sub> and CH<sub>4</sub> from small wetland lakes in western Siberia, *Tellus, Ser. B Chem. Phys. Meteorol.*, 59(5), 788–796, doi:10.1111/j.1600-0889.2007.00301.x, 2007.
- 720 Ruskeeniemi, T., Engström, J., Lehtimäki, J., Vanhala, H., Korhonen, K., Kontula, A., Claesson Liljedahl, L., Näslund, J. O. and Pettersson, R.: Subglacial permafrost evidencing re-advance of the Greenland Ice Sheet over frozen ground, *Quat. Sci. Rev.*, 199, 174–187, doi:10.1016/j.quascirev.2018.09.002, 2018.
- Sharp, M., Parkes, J., Cragg, B., Fairchild, I. J., Lamb, H. and Tranter, M.: Widespread bacterial populations at glacier beds and their relationship to rock weathering and carbon cycling, *Geology*, 27(2), 107–110, doi:10.1130/0091-7613(1999)027<0107:WBPAGB>2.3.CO;2, 1999.
- 725 Solinst: Solinst Technical Bulletin: Understanding pressure sensor drift, 2017.
- St Pierre, K. A., St Louis, V. L., Schiff, S. L., Lehnert, I., Dainard, P. G., Gardner, A. S., Aukes, P. J. K. and Sharp, M. J.: Proglacial freshwaters are significant and previously unrecognized sinks of atmospheric CO<sub>2</sub>, *Proc. Natl. Acad. Sci.*, 116(36), 17690–17695, doi:10.1073/pnas.1904241116, 2019.
- 730 [Stibal, M., Wadham, J. L., Lis, G. P., Telling, J., Pancost, R. D., Dubnick, A., Sharp, M. J., Lawson, E. C., Butler, C. E. H., Hasan, F., Tranter, M. and Anesio, A. M.: Methanogenic potential of Arctic and Antarctic subglacial environments with](#)

- [contrasting organic carbon sources, \*Glob. Chang. Biol.\*, 18\(11\), 3332–3345, doi:10.1111/j.1365-2486.2012.02763.x, 2012.](#)
- Tipple, B. J., Meyers, S. R. and Pagani, M.: Carbon isotope ratio of Cenozoic CO<sub>2</sub>: A comparative evaluation of available geochemical proxies, *Paleoceanography*, 25(3), 1–11, doi:10.1029/2009pa001851, 2010.
- 735 Tranter, M.: Geochemical Weathering in Glacial and Proglacial Environments, in *Surface and Ground Water, Weathering, and Soils: Treatise on Geochemistry*, vol. 5, edited by J. I. Drever., 2005.
- Upton, B. G. J., Emeleus, C. H., Heaman, L. M., Goodenough, K. M. and Finch, A. A.: Magmatism of the mid-Proterozoic Gardar Province, South Greenland: Chronology, petrogenesis and geological setting, *Lithos*, 68(1–2), 43–65, doi:10.1016/S0024-4937(03)00030-6, 2003.
- 740 Urra, A., Wadham, J., Hawkings, J. R., Telling, J., Hatton, J. E., Yde, J. C., Hasholt, B., van As, D., Bhatia, M. P. and Nienow, P.: Weathering Dynamics Under Contrasting Greenland Ice Sheet Catchments, *Front. Earth Sci.*, 7(November), doi:10.3389/feart.2019.00299, 2019.
- de Visscher, A., de Pourcq, I. and Chanton, J.: Isotope fractionation effects by diffusion and methane oxidation in landfill cover soils, *J. Geophys. Res. Atmos.*, 109(18), 1–8, doi:10.1029/2004JD004857, 2004.
- 745 Wadham, J. L., Tranter, M., Tulaczyk, S. and Sharp, M.: Subglacial methanogenesis: A potential climatic amplifier?, *Global Biogeochem. Cycles*, 22(December 2007), 1–16, doi:10.1029/2007GB002951, 2008.
- [Wadham, J. L., Tranter, M., Skidmore, M., Hodson, A. J., Priscu, J., Lyons, W. B., Sharp, M., Wynn, P. and Jackson, M.: Biogeochemical weathering under ice: Size matters, , 24\(December 2009\), doi:10.1029/2009GB003688, 2010.](#)
- [Wadham, J. L., Hawkings, J. R., Tarasov, L., Gregoire, L. J., Spencer, R. G. M., Gutjahr, M., Ridgwell, A. and Kohfeld, K. E.: Ice sheets matter for the global carbon cycle, \*Nat. Commun.\*, 10\(1\), doi:10.1038/s41467-019-11394-4, 2019.](#)
- [van de Wal, R. S. W. and Russell, A. J.: A comparison of energy balance calculations, measured ablation and meltwater runoff near Sondre Stromfjord, West Greenland, \*Glob. Planet. Change\*, 9, 29–38 \[online\] Available from: <http://www.phys.uu.nl/~wal/research/papers/walandrus94.pdf>, 1994.](#)
- Walker, J. C. G., Hays, P. B. and Kasting, J. F.: A negative feedback mechanism for the long-term stabilization of earth's surface temperature, *J. Geophys. Res.*, 86(1), 9776–9782, 1981.
- 755 Warren, C. R. and Glasser, N. F.: Contrasting response of south Greenland glaciers to recent climatic change, *Arct. Alp. Res.*, 24(2), 124–132, doi:10.2307/1551532, 1992.
- Whiticar, M. J.: Carbon and hydrogen isotope systematics of bacterial formation and oxidation of methane, *Chem. Geol.*, 161, 291–314, 1999.
- 760 Whiticar, M. J. and Schoell, M.: Biogenic methane formation in marine and freshwater environments: CO<sub>2</sub> reduction vs.

acetate fermentation- Isotope evidence, *Geochim. Cosmochim. Acta*, 50, 693–709, 1986.

Wimpenny, J., James, R. H., Burton, K. W., Gannoun, A., Mokadem, F. and Gislason, S. R.: Glacial effects on weathering processes: New insights from the elemental and lithium isotopic composition of West Greenland rivers, *Earth Planet. Sci. Lett.*, 290(3–4), 427–437, doi:10.1016/j.epsl.2009.12.042, 2010.

765 Wimpenny, J., Burton, K. W., James, R. H., Gannoun, A., Mokadem, F. and Gislason, S. R.: The behaviour of magnesium and its isotopes during glacial weathering in an ancient shield terrain in West Greenland, *Earth Planet. Sci. Lett.*, 304(1–2), 260–269, doi:10.1016/j.epsl.2011.02.008, 2011.

Winsor, K., Carlson, A. E. and Rood, D. H.: <sup>10</sup>Be dating of the Narsarsuaq moraine in southernmost Greenland: Evidence for a late-Holocene ice advance exceeding the Little Ice Age maximum, *Quat. Sci. Rev.*, 98, 135–143, 770 doi:10.1016/j.quascirev.2014.04.026, 2014.

Yde, J. C., Knudsen, N. T., Hasholt, B. and Mikkelsen, A. B.: Meltwater chemistry and solute export from a Greenland Ice Sheet catchment, Watson River, West Greenland, *J. Hydrol.*, 519(PB), 2165–2179, doi:10.1016/j.jhydrol.2014.10.018, 2014.

**Deleted:** World Meteorological Organization: Manual on Stream Gauging. Volume I: Fieldwork, 2010.

775 **Table 1. Mineral weathering reactions and impacts on dissolved CO<sub>2</sub> concentrations.**



<i>Eq.</i>	<i>Mineral</i>	<i>Acid</i>	<i>Abbreviation<sup>1</sup></i>	<i>Reaction</i>	<i>Impact on CO<sub>2</sub></i>
(1)	Carbonate	Carbonic	Carbc <sub>A</sub>	$(Ca, Mg)CO_3 + H_2O + CO_2 \rightarrow (Ca^{2+}, Mg^{2+}) + 2HCO_3^-$	CO <sub>2</sub> sink
(2)		Sulfuric	Carbs <sub>SA</sub>	$2(Ca, Mg)CO_3 + H_2SO_4 \rightarrow 2(Ca^{2+}, Mg^{2+}) + SO_4^{2-} + H_2O + CO_2$	CO <sub>2</sub> source
(3a)	Silicate	Carbonic	Silc <sub>A</sub>	$(Ca, Mg)Al_2Si_2O_8 + 2CO_2 + 3H_2O \rightarrow (Ca^{2+}, Mg^{2+}) + 2HCO_3^- + Al_2Si_2O_5(OH)_4$	CO <sub>2</sub> sink
(3b)				$(Na, K)AlSi_3O_8 + CO_2 + 5.5H_2O \rightarrow (Na, K) + HCO_3^- + 0.5Al_2Si_2O_5(OH)_4 + 2H_4SiO_4$	CO <sub>2</sub> sink
(4a)		Sulfuric	Sils <sub>SA</sub>	$(Ca, Mg)Al_2Si_2O_8 + H_2SO_4 + H_2O \rightarrow (Ca^{2+}, Mg^{2+}) + SO_4^{2-} + Al_2Si_2O_5(OH)_4$	No impact
(4b)				$2(Na, K)AlSi_3O_8 + H_2SO_4 + 9H_2O \rightarrow 2(Na^+, K^+) + SO_4^{2-} + Al_2Si_2O_5(OH)_4$	No impact

<sup>1</sup>Abbreviations are based first on the mineral class (carbonate = carb, silicate = sil) and then on the acid (carbonic acid = CA, sulfuric acid = SA)

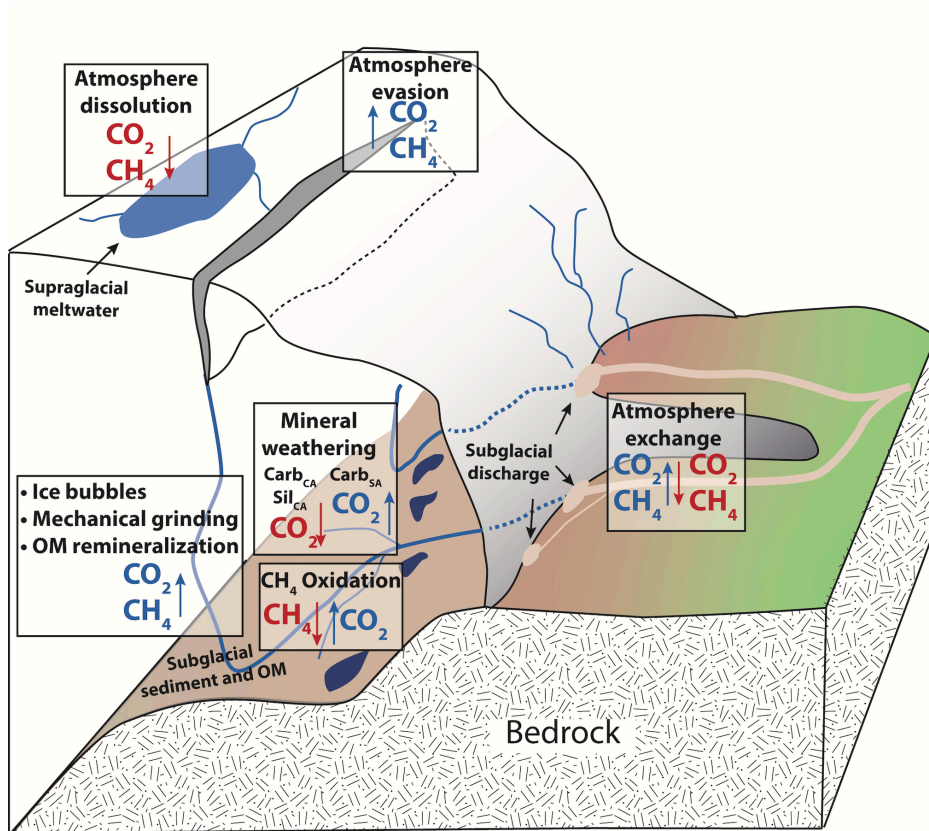
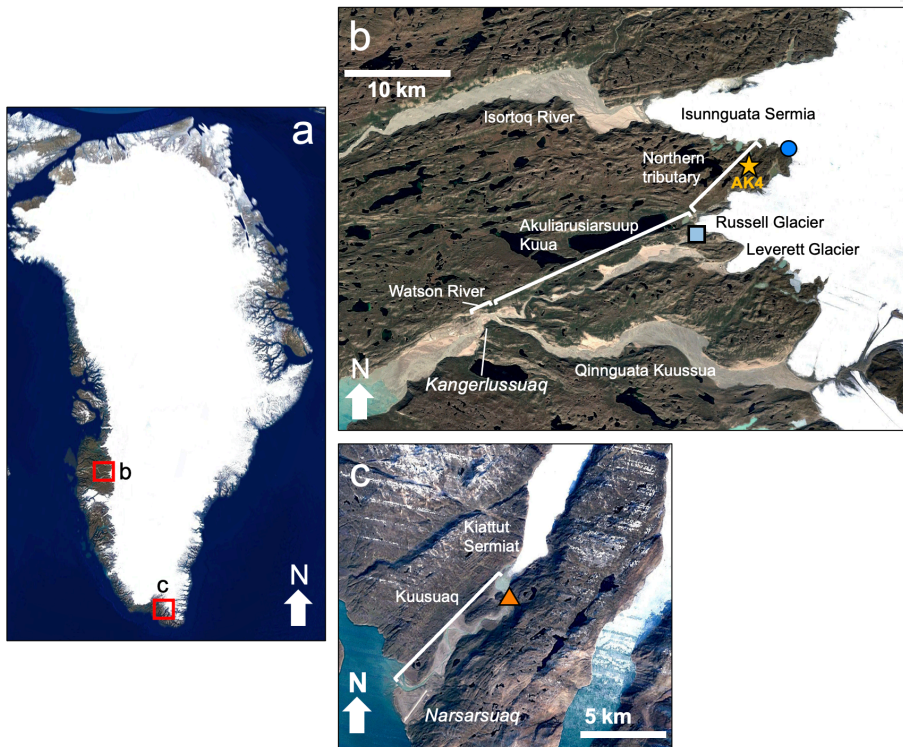
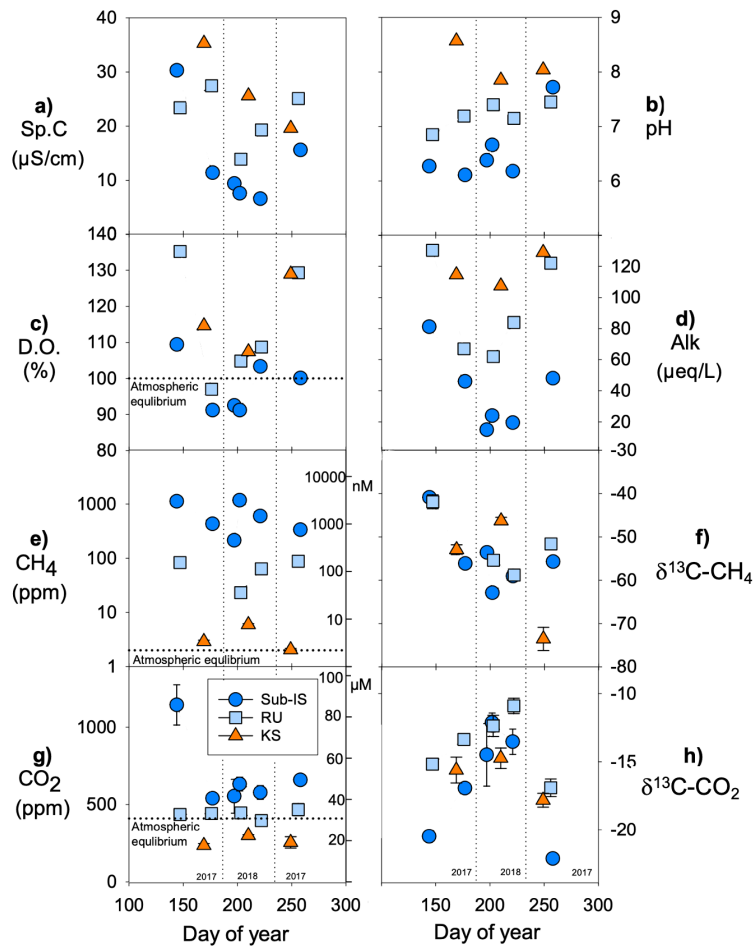


Figure 1: Conceptual diagram of subglacial sources and sinks of  $\text{CO}_2$  and  $\text{CH}_4$ . Arrows indicate the direction of fluxes. Boxes represent processes, and sources of gases to subglacial meltwaters are indicated by blue text while sinks of gases to subglacial meltwater are indicated by red text. Gas bubbles, mechanical grinding, and OM remineralization are grouped because all are  $\text{CO}_2$  and  $\text{CH}_4$  sources.

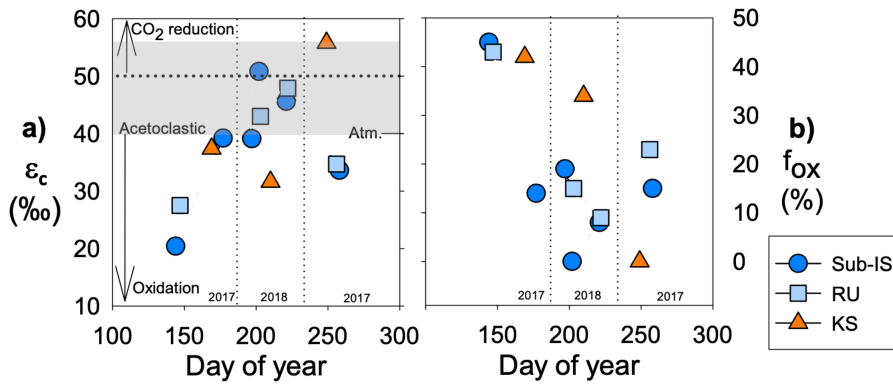
785



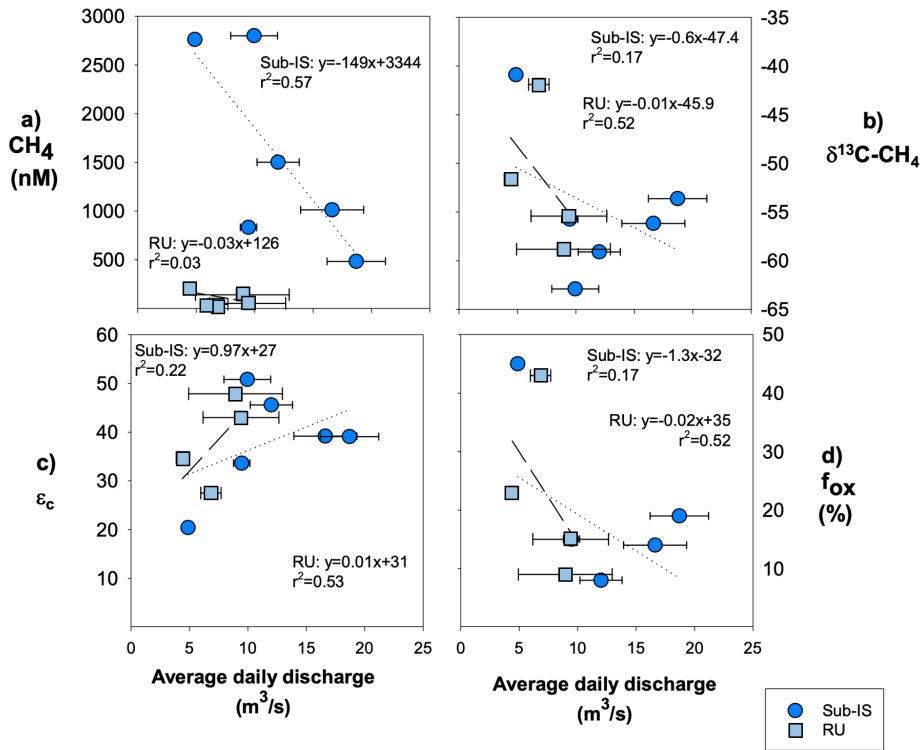
790 **Figure 2.** Google Earth satellite images of study locations in a) Greenland including b) locations near the town of Kangerlussuaq, including the sub-Isunnguata water sampling location (dark blue circle) and Russell water sampling location (light blue square). The gold star represents the location of AK4, where proglacial river discharge records were collected. (c) Location of Kiattut Sermiat site (orange triangle) near the town of Narsarsuaq in southern Greenland where water samples were collected.



795 **Figure 3.** Chemical parameters at Isunnguata (IS), Russell (RU) and Kiattut Sermiat (KS) subglacial water sampling sites versus  
 day of year for a) specific conductivity (Sp.C), b) pH, c) dissolved oxygen (D.O.) percent saturation, d) alkalinity (Alk), e) measured  
 CH<sub>4</sub> concentrations (left y-axis in ppm and right y-axis in nM), f)  $\delta^{13}\text{C}\text{-CH}_4$  values, g) measured CO<sub>2</sub> concentrations (left y-axis in  
 ppm and right y-axis in  $\mu\text{M}$ ), and h)  $\delta^{13}\text{C}\text{-CO}_2$  values. Atmospheric equilibrium concentrations are indicated by dashed lines and  
 taken as 1.9 ppm for CH<sub>4</sub> and 410 ppm for CO<sub>2</sub>. Error bars on CH<sub>4</sub> and CO<sub>2</sub> concentrations and stable isotopic compositions  
 800 represents the standard deviation of replicates and are smaller than symbols for some data points.



805 **Figure 4.** CH<sub>4</sub> dynamics over the course of the 2017 and 2018 melt seasons including a) the carbon fractionation factor ( $\epsilon_c$ ) between dissolved CO<sub>2</sub> and CH<sub>4</sub> and b) the fraction of CH<sub>4</sub> oxidized ( $f_{ox}$ ) for sub-Isunnguata (IS), Russell (RU) and Kiattut Sermiat (KS) samples. Fields of  $\epsilon_c$  representing methanogenesis and oxidation values are based on Whiticar (1999). Values of  $\epsilon_c$  between approximately 40 and 55 (gray shaded region in panel a) are produced for methanogenesis via acetate fermentation, while CO<sub>2</sub> reduction produces values between approximately 50 and 90. Lower values result from a predominant isotopic signature of CH<sub>4</sub> oxidation. Atmospheric input without additional alteration of CO<sub>2</sub> or CH<sub>4</sub> isotopic systematics results in a  $\epsilon_c$  value of approximately 40.



810

Figure 5. Relationships between average daily discharge and CH<sub>4</sub> dynamics including a) CH<sub>4</sub> concentrations, b) δ<sup>13</sup>C-CH<sub>4</sub>, c) ε<sub>c</sub>, and d) f<sub>ox</sub> for Isunnguata (IS) and Russell (RU) samples. Regressions are shown by dotted lines for Isunnguata and dashed lines for Russell samples. Horizontal error bars represent the standard deviation of average daily discharge for days samples were collected and are smaller than symbols for some data points.

815

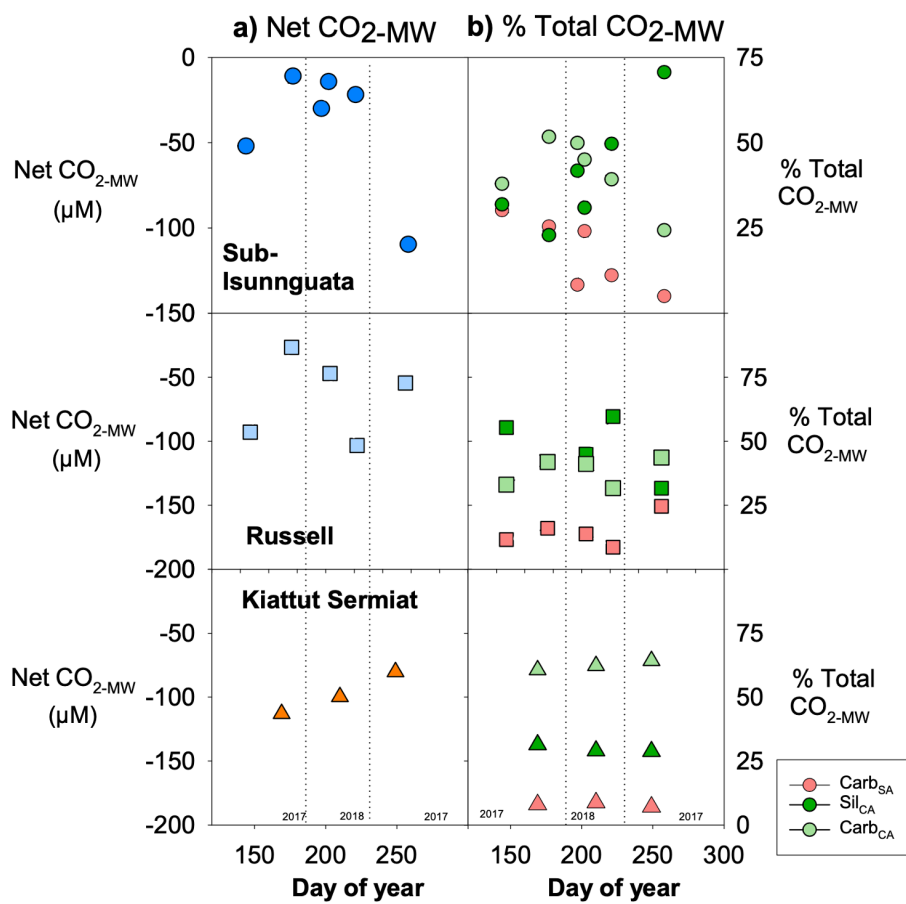
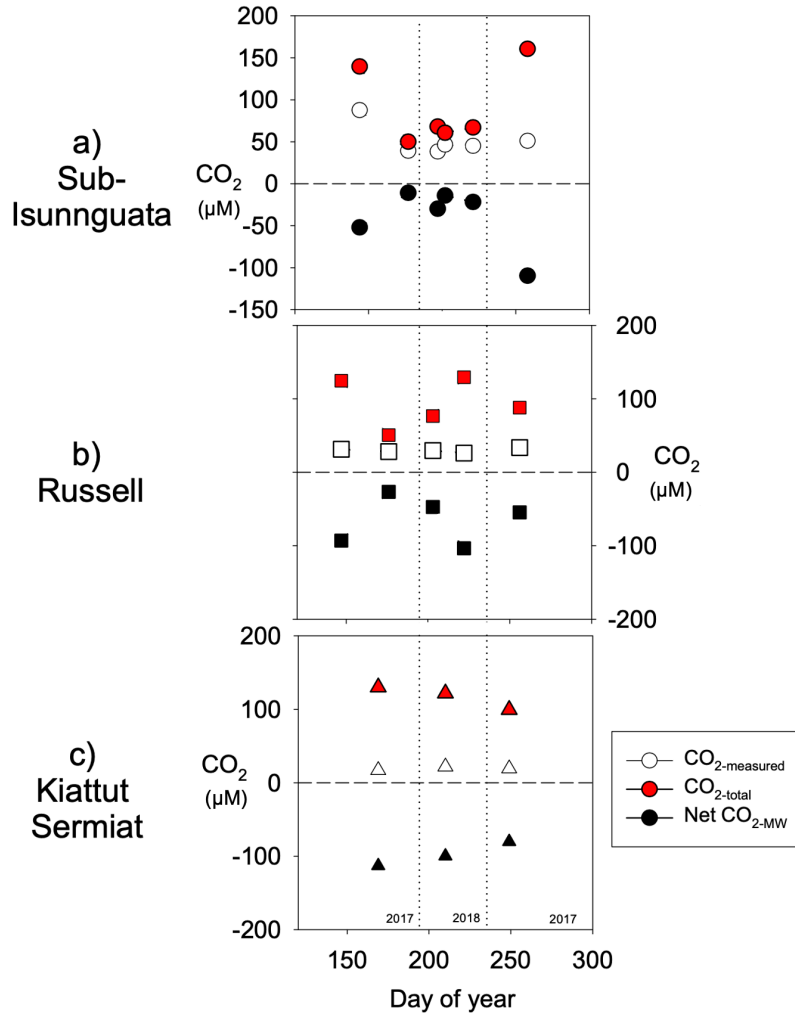


Figure 6. Mineral weathering model results in a) net impact of mineral weathering reactions on CO<sub>2</sub> (Net CO<sub>2-MW</sub>; Eq. 7) for Isunnguata, Russell, and Kiattut Sermiat subglacial discharge sites (where negative values of Net CO<sub>2-MW</sub> indicate net sequestration of CO<sub>2</sub> due to mineral weathering), and b) the proportional contribution of each mineral weathering reaction to the total change in CO<sub>2</sub> (% Total CO<sub>2-MW</sub> Eq. 9a-9c).

820



825 Figure 7. Calculated CO<sub>2</sub>-total values for a) sub-Isunnguata, b) Russell, and c) Kiattut Sermiat subglacial discharge against day of the year.



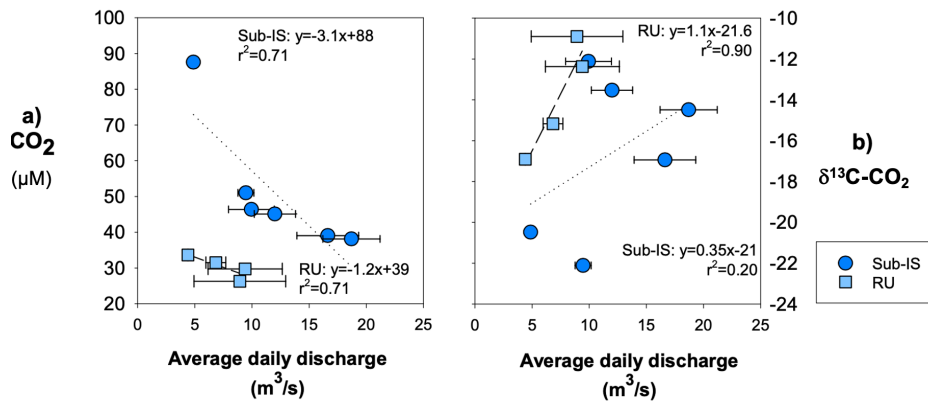


Figure 8. Relationships between average daily discharge a) CO<sub>2</sub> concentrations, and b) δ<sup>13</sup>C-CO<sub>2</sub>. Regressions are shown by dotted lines for sub-Isunnguata and dashed lines for Russell samples. Horizontal error bars represent the standard deviation of average daily discharge for days samples were collected and are smaller than symbols for some data points.

830

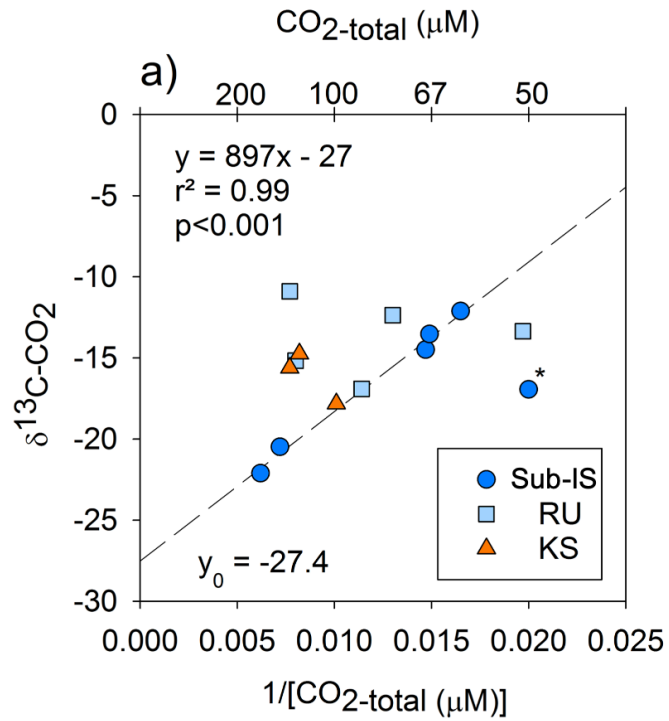


Figure 9. Keeling plot indicating correlations between the magnitude of CO<sub>2</sub>-total and δ<sup>13</sup>C-CO<sub>2</sub> and for sub-Isunnguata (sub-IS), Russell (RU) and Kiattut Sermiat (KS) samples. Asterisk denotes the outlier not included in the regression between CO<sub>2</sub>-total and δ<sup>13</sup>C-CO<sub>2</sub> for sub-Isunnguata samples. The plotted regression line was constructed using the sub-IS samples only.